1. Final report

1.1 Project details

Project title	Synchronous condenser applications in low inertia systems
Project identification (program abbrev. and file)	EUDP 64018-0002 ForskEL-projekt 2014-1-12196
Name of the programme which has funded the project	ForskEL/EUDP
Project managing company/institution (name and address)	Technical University of Denmark Elektrovej building 325, Center for Electric Power and Energy Kgs. Lyngby 2800
Project partners	Siemens Danmark
CVR (central business register)	30060946
Date for submission	4 Sept 2019

1.2 Short description of project objective and results

In this project, Siemens A/S and DTU set out to investigate the characteristics of a renewable-energy-based power system and identify the potential and requirements for synchronous condensers in the future. The collaboration will generate deeper knowledge on synchronous condensers for renewable energy systems, and provide methods in d sign and utilization of synchronous condensers with respect to grid requirements.

I dette projekt undersøger DTU og Siemens Danmark A / S i samarbejde egenskaberne ved et vedvarende energibaseret elsystem og identificerer potentialet og kravene til synkrone kondensatorer i fremtiden. Samarbejdet vil skabe dyb viden om de dynamiske egenskaber ved konverterbaserede vedvarende energisystemer og tilvejebringe metoder i design og anvendelse af synkrone kondensatorer med hensyn til netværksydelse.

1.3 Executive summary

Synchronous condensers are considered as an essential component to secure a renewa-ble energy system. DTU aims to establish a research and experimental hub on renewable energy integration. Siemens Danmark aims to build a global knowledge center on syn-chronous condensers. The objective of the project is to quantify the impact of a convert-er-based platform on system frequency and voltage characteristics during transients, namely the system frequency inertia and short-circuit power. The project also aims to determine the optimal design and parameter settings for SCs to provide essential grid services in renewable-based systems, to improve the reliability of protection and to set the system controls during normal and emergency situations, thereby improving system security. The system of analysis will be developed from the current Danish grid to look towards a future scenario with 100% renewable energy in 2035.

The project helps to establish a global competence and knowledge centre in Denmark on the application and research of synchronous condensers to enable a higher penetration of renewable energy in the system and to strengthen the Danish position internationally in terms of practice and knowledge of renewable integration, as well as create new knowledge-based jobs in the renewable era. Siemens A/S and DTU are ensuring that Denmark maintains a leading position in the integration of renewable energy.

1.4 Project objectives

with the increasing penetration of renewable energy sources, the system's properties may be largely affected by the retirement of traditional synchronous machines, and the electric system responses during transients may be significantly affected. Investigations are required to quantify those impacts and provide solutions to support system operations and security.

Given the characteristics of synchronous condensers, it may play a crucial role in a future system with extensive use of converter based technologies. However, though the application of SCs can be found in such a system, the implementation should be based on detailed studies, including quantitative analysis of the services provided by the renewable generation systems, the advances in SCs with respect to different designs, and various case studies for validation.

The objective of the project is to quantify the impact of a converter-based platform on system frequency and voltage characteristics during transients, namely the system frequency inertia and short-circuit power. The project also aims to determine the optimal design and parameter settings for SCs to provide essential grid services in renewable-based systems, to improve the reliability of protection and to set the system controls during normal and emergency situations, thereby improving system security. The system of analysis will be developed from the current Danish grid to look towards a future scenario with 100% renewable energy in 2035.

In addition, the project helps to establish a global competence and knowledge centre in Denmark on the application and research of synchronous condensers to enable a higher penetration of renewable energy in the system and to strengthen the Danish position internationally in terms of practice and knowledge of renewable integration, as well as create new knowledge-based jobs in the renewable era.

The project will set up an experimental platform in PowerlabDK using a real-time digital simulator (RTDS) for testing and validation of the control of synchronous condensers.

1.5 Project results and dissemination of results

This section details the key findings from the project. Not all results are included in the final report due to page limits. Further information can be found in the disseminations.

1.5.1 Frequency response characterization and enhancement

1.5.1.1 Fundamentals of power system inertia

Inertia reduction due to high-level penetration of converter interfaced components may result in frequency stability issues. The work proposes and analyzes different strategies using synchronous condenser (SC), synthetic inertia (SI) of wind power plant, and their combination for frequency stability enhancement in low inertia systems under various scenarios and wind conditions. The simplified Western Danish power system simulated in real time digital simulator (RTDS) is used as a test system of low inertia to demonstrate the effectiveness of the strategies. The comparative results show that the combination of SC and SI offers a better improvement not only on frequency stability (rate of change of frequency and frequency deviation) but also on the system synchronism under various operating conditions.

System inertia is defined as the resistance to changes in the system frequency by storing/injecting kinetic energy from/to the system during power imbalance, which comes from synchronously connected rotating machines. The kinetic energy of a system is calculated as

$$E_{rot} = \sum_{i=1}^{n} \left(\frac{1}{2} J_i \omega_{mi}^2 \right)$$

where J_i and ω_{mi} are the moment of inertia and the rotational speed of the *i*-th rotating machine, respectively; and *n* is the number of rotating machines.

The system inertia constant is determined by the ratio of total stored kinetic energy in MJ at a synchronous speed ω_{sm} to the MVA rating of the base system as

$$H_{sys} = \frac{E_{rots}}{S_{base}} = \frac{\omega_{sm}^2}{2S_{base}} \sum_{i=1}^{n} (J_i)$$

The initial ROCOF that is determined by the size of the power imbalance and the system inertia is expressed by

$$ROCOF = \frac{f_0}{2H_{sys}} \frac{\Delta P}{S_{base}} = \frac{f_0 \Delta P}{2E_{rot}}$$

where ΔP is the disturbance size, f_0 is the nominal system frequency. The initial ROCOF is decided by the system inertia or the total kinetic energy and the disturbance size.

Since SC is a rotating machine, it can provide an inherently inertial response due to the electromagnetic coupling with the grid and the electromechanic coupling with the speed. The kinetic energy stored in its rotating mass can naturally counteract any frequency change during disturbances.

Unlike synchronous generators that can naturally inject or absorb kinetic energy stored in their rotating mass during disturbances, variable-speed wind power plants (WPPs) do not have that ability even they have rotating masses. Hence, a proper controller needs to be implemented to take advantage of the rotating masses.

The damping effect from synchronous condenser against the system frequency change comes with the design and the passivity of the operation. When there is sudden change in system frequency (or angle change due to faults), the angle difference between the terminal voltage and rotor position of synchronous condenser will break the power/speed balance, resulting in immediate reaction through injecting or absorbing active power to or from the grid to retain synchronism. When the terminal voltage angle fastly goes up and down, condenser rotor angle will be affected and results in oscillations. Due to the passivity of operation, this oscillation is mostly against the direction of the change from the system thereby SC provides damping effect to the grid.

1.5.1.2 Synthetic inertia control design

The future system frequency is determined by asynchronous (converter based, induction generators) generation as well as synchronous (synchronous machines) generation. Therefore, it is important that converter control effect and potential on frequency support and inertia provision is clearly understood, before further investigation of the system inertia. In the project, effort was spent on developing inertia control of converters (from wind power

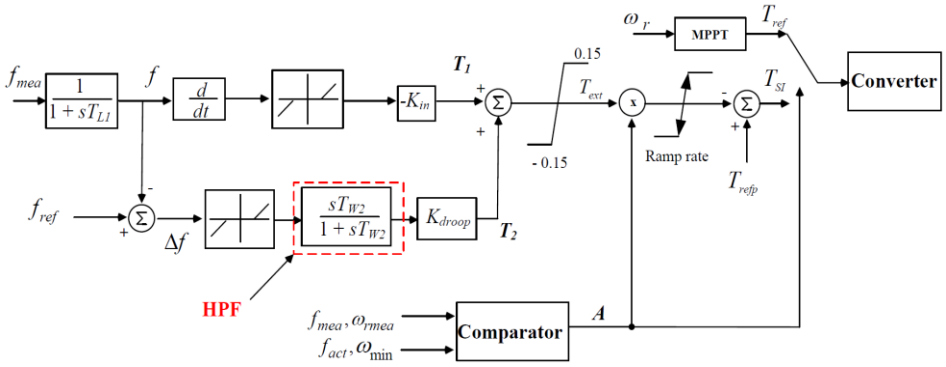

Figure 1. The proposed synthetic inertia controller.

generation). The idea of the proposed control method is changing the torque reference which in turn changes the power command of WPP during frequency excursions. Fig. 1 shows the proposed synthetic inertia controller that includes two control loops, the first one takes df/dt

as the input to create an additional signal T_1 works as inertial response of synchronous generator, the second one generates an extra signal T_2 from frequency deviation input, reacting like the droop control or fast frequency response. Whenever system frequency changes from the nominal value, the torque command will be changed by the contribution of the SI controller.

As can be seen in Fig. 1, the system frequency is firstly measured and filtered by a low pass filter to eliminate the measurement noise. Then, a deadband (±0.015 Hz) is deployed to avoid the participation of the synthetic inertia control to reduce the bandwidth avoiding pulsations in the drive-train of the wind turbine in the normal operating condition. The first loop is in charge of additionally providing an offset signal T_1 that is proportional to df/dt. The second loop is responsible for supplying an additional torque signal T_2, which is proportional to the frequency deviation from its nominal value.

A high pass filter (HPF) is applied to guarantee the turbine can recover the operating speed when the system frequency reaches a new steady-state operating point. T_{W2} of HPF is selected to decide how long the second loop output can contribute to frequency control during disturbances.

In order to avoid competing control effect, the proposed method switches the reference from T_{ref} of MPPT control to T_{SI} of the proposed scheme during the inertial response. The steady state output of SI can be expressed as follows

$$T_{SI} = K_{in}\frac{df}{dt} - K_{droop}\Delta f + T_{refp}$$

Where T_{refp} is the reference from MPPT corresponding to pre-disturbance rotor speed that is stored in the system data.

It is important to select properly the values of K_{in} and K_{droop}. Otherwise, it may cause a poor performance for the controller. K_{in} is proportional to df/dt control loop, a high K_{in} value may result in over-ramp up a limit of turbine speed that can destroy the mechanical part of the turbine. K_{droop} is the gain of Δf control loop, a high K_{droop} selection may lead to a large turbine speed drop that makes the turbine unable to recover a secure operating point after disturbances. K_{droop} is selected based on the droop characteristics of SG (from 2%-12%). An optimal combination of the two gains can achieve a good performance for SI on the frequency stability improvement. A ramp rate limit is added to prevent the immediate on/off activated signal in case reaching the minimum allowable rotor speed limit. A proper value of the ramp rate limit makes the transfer period smoother and less mechanical stress on the turbine and rotor.

An activation scheme combined with a minimum allowable rotor speed check is implemented on this control strategy to guarantee that the rotor does not operate below its the minimum allowable speed that may stall the turbine. The activation scheme can be described by

$$if \begin{cases} f_{\min} \le f_{mea} \le f_{\max} : \ set\ A = 0 \\ \omega_{rmea} \le \omega_{\min} \end{cases}$$

$$else: \ set\ A = 1$$

The SI controller will not be activated when the system frequency is within the allowable operating range and the rotor speed is equal or less than its minimum allowable speed.
Here we proposed a combination of SC and SI of WPPs to offer an optimal performance for the frequency stability enhancement. While SC can quickly respond to frequency change

based on ROCOF due to its electromagnetic connection at the onset of the disturbance, SI of WPPs will support afterwards for counteracting the frequency deviation and compensating kinetic power recovery for SC which SC needs to return its pre-disturbance speed after participating in frequency control. SI contribution can be controlled to have fast contribution when the disturbance occurs and recover a bit slower to give time for primary control react. As a result, a combination of SC and SI can not only help system frequency improve ROCOF and the frequency deviation, but also make system frequency much stronger during frequency excursions.

1.5.1.3 Case studies

To verify the proposed control method, the future Western Danish renewable-based system which uses a majority of converter-interfaced generation like wind power plants and HVDC interconnections, is used as a typical low inertia system as shown in Fig. 2.

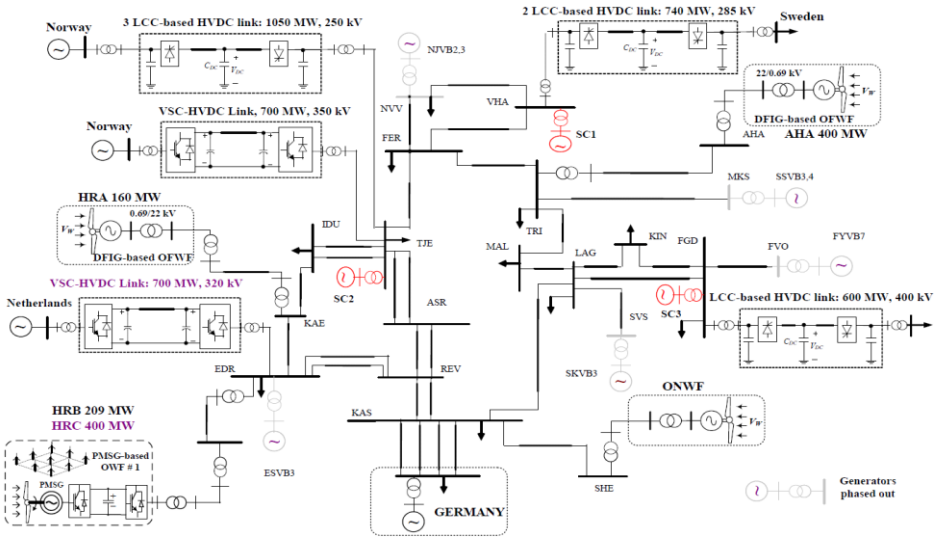

Figure 2. The future western Danish renewable system.

Different future scenarios of the DK1 system based on the data provided by the local transmission operator are studied in order to examine the proposed method under various disturbances/faults as shown in Fig. 3. SI is implemented for 2 OFWFs which are located at AHA and HRB, C.

1) Base case

This case is based on the DK1 system data in 2020, all 5 local SGs (873 MW central produc-

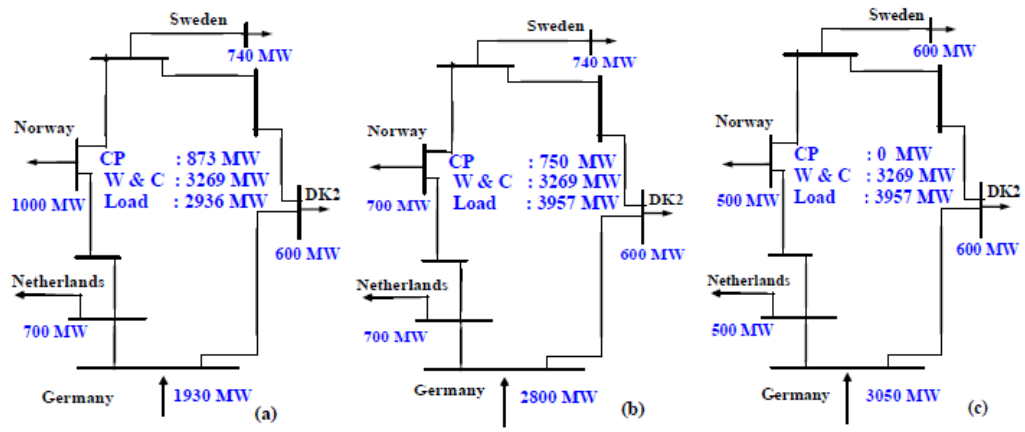

Figure 3. Future scenarios of the DK1 system (CP: central production, W & C: wind and coastal production). (a) Base case. (b) HLHW with 3 SGs. (c) HLHW no SGs.

tion) are operating with the power flows as shown in Fig. 3(a).

To verify the contribution of SC to the frequency stability improvement, the system response during 200 MW load located at MAL increases at t = 1 s is investigated in this case with SCs in red and without SCs in black as shown in Fig. 4. With SC in operation, the system fre-

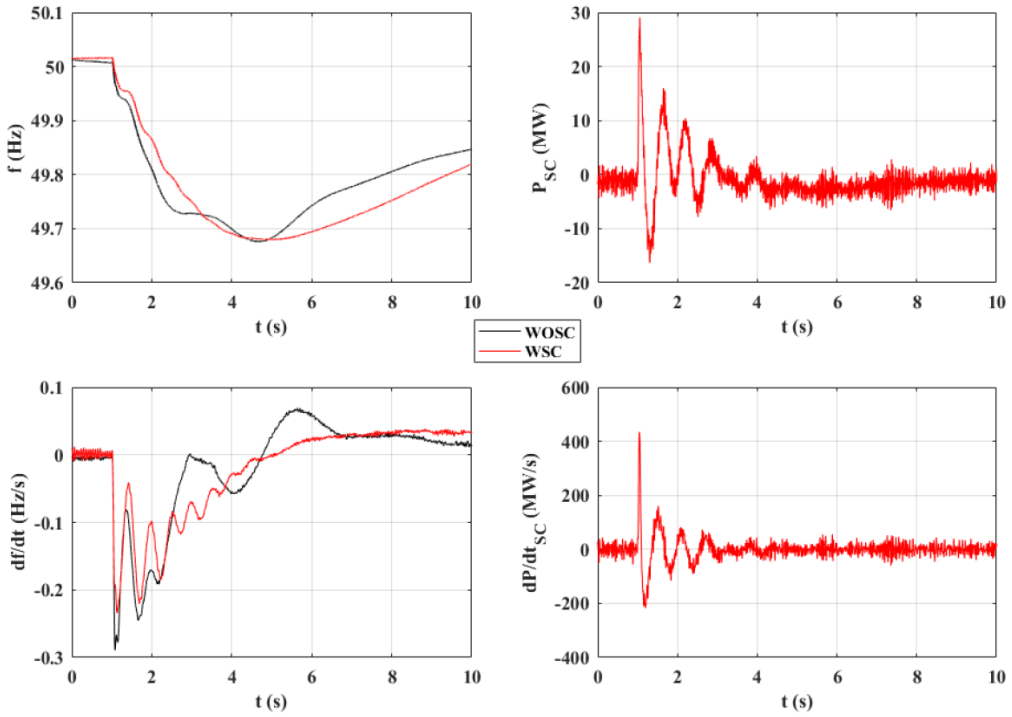

Figure 4. System frequency, ROCOF, and SC responses during the disturbance.

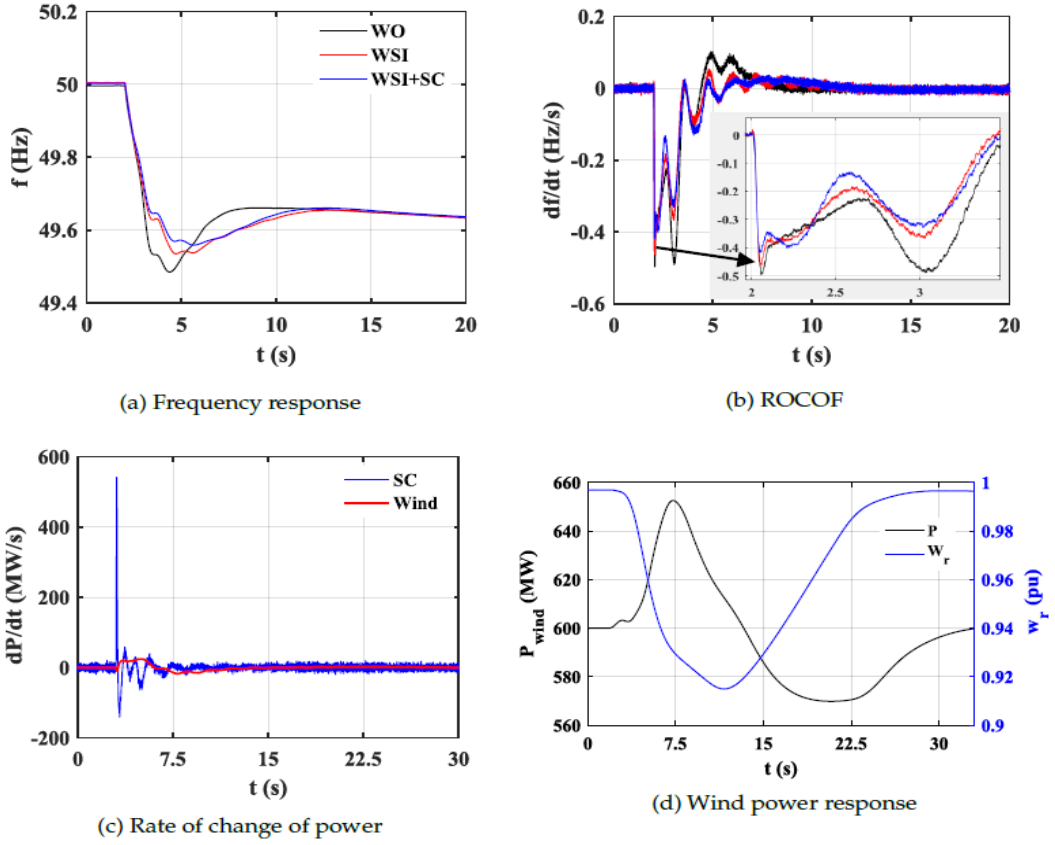

Figure 5. System responses during 10% load increase disturbance of HWHL 3 SGs in operation.

quency response is much smoother and stronger. Additionally, ROCOF is significantly improved nearly 0.29 Hz/s compared to around 0.233 Hz/s without SC case. It is noteworthy that when the disturbance occurs SC immediately releases the electric energy to counteract the frequency drop with nearly 420 MW/s active power gradient as shown in the last sub-plot of Fig. 4.

2) High wind and high load with 3 online SGs

Another scenario is investigated in this case where the load is assumed to use in 2050 estimated 1% increase per year based on the base-case load and the wind speed reaches the rated speed at 12 m/s so that WPPs are operating at their rated power output. There is three committed SGs in operation with the power flow as shown in Fig. 3(b).

A 10% load increase incident at bus MAL occurs at t = 2 s. The system response during the incident is illustrated in Fig. 5 with the black for without any inertia support, the red for with SI controller, and the blue for with SC combined SI. It can be seen clearly that SI can improve significantly frequency nadir from 49.45 Hz to 49.55 Hz, whereas SCs combined SI can enhance both frequency deviation and ROCOF.

By comparing ROCOF response, without any inertia support the system frequency is much more vulnerable, ROCOF reaches a maximum value twice at around 2.1 s and nearly 3.1 s as zoomed in Fig. 5(b). It can be explained that at the first onset of the incident, the three online synchronous generators and the German generator rapidly release their kinetic energy to against frequency change that helps ROCOF increasing after experiencing a first maximum value around 0.5 Hz/s. However, this kinetic energy is insufficient to help ROCOF recover completely, a second maximum ROCOF is at around 3.1 s as its consequence for a low inertial response of the system as seen obviously in Fig. 5(b) with the black curve.

This issue is dealt with SC and SI in operation case where ROCOF is quickly settled down instead of undergoing a large oscillation of the WO case. The inertia support of an SC and SI combination can be described as follows: at first few seconds following the disturbance, SC's rotating energy is released in order to support the inertial response that helps ROCOF improved, SI responds afterwards to increase temporarily WPP power output for counteracting the frequency drop as well as compensating for SC's rotating energy recovery. It can be seen much more clearly about the response time that shows how fast they react from the active power gradient (dP/dt) plots of SC and WPP in Fig. 5(c). Consequently, the combination of SI and SC results in an efficient enhancement of the frequency stability in term of frequency nadir and ROCOF. As expected, WPP can recover the pre-disturbance operating speed when the system frequency reaches a new equilibrium as shown in Fig. 5(d).

3) High wind and high load without SGs

A scenario with all synchronous generators phased out (no central production) is studied in this case with the power flow as shown in Fig. 3(c). In this situation, the system operates in a very low inertia constant and relies mainly on the German interconnection. The frequency is measured at three locations KAS, LAG, and FER to witness the frequency synchronization when the system operates in a low inertia condition.

Load increase disturbance: The same 10% load increase disturbance size occurs. As can be seen clearly from Fig. 6, the system frequency without SC+SI (WO) undergoes a huge oscillation and gets unstable after around 5 s because only the German side provided inertial support is insufficient for the frequency recovery in this operating condition.

It is worth to be mentioned here is the frequency behaviour in different locations of the system. A reverse oscillation occurs with the frequency at KAS compared to that of FER and LAG. With the combination of SC and SI in service, the system stays in synchronism and becomes stable after approximately 5 s as seen in Fig. 6(c). It can be explained that at the onset of the incident, the inertial response from the German side and SCs tries to restrain the frequency change, after that the inertia support from SI of WPPs and primary control help the system frequency recovery and stable. Only SI in operation is not fast enough for the frequency support in this low inertia condition, which leads to an asynchronism of frequencies at different parts and a large oscillation before getting stable on the system frequency, as shown in Fig. 6(b).

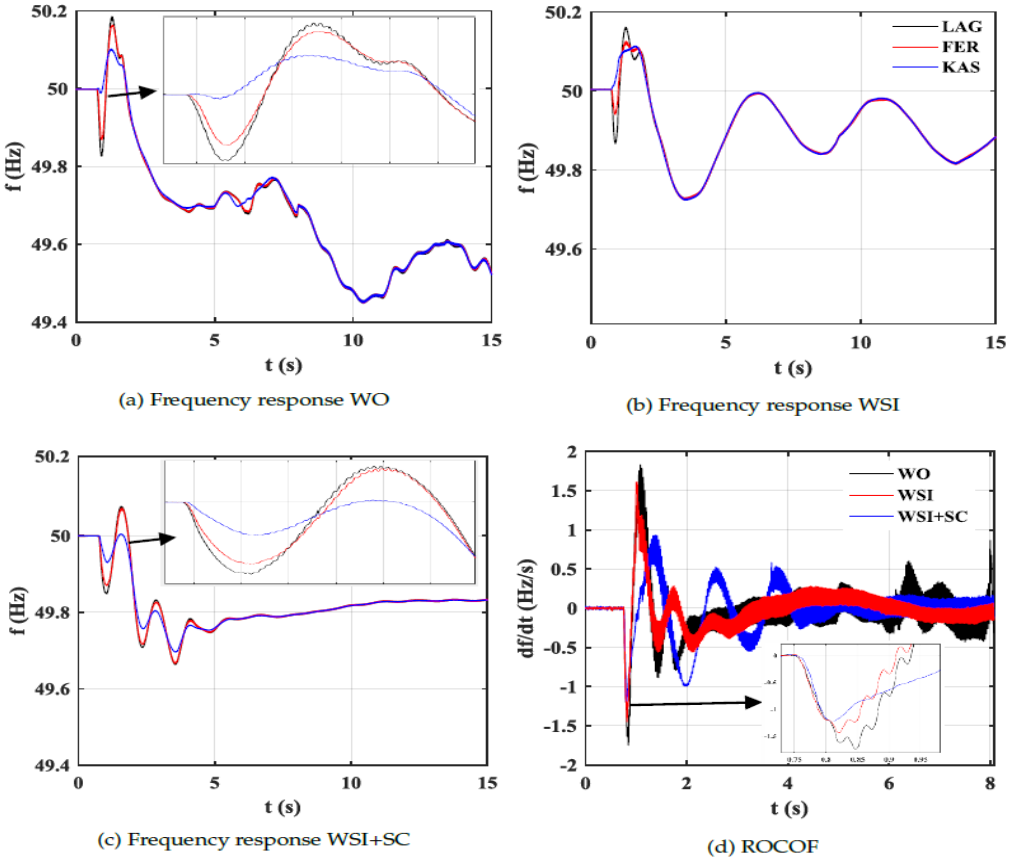

Figure 6. System responses during 10% load increase disturbance of HWHL no local SGs in operation.

It should be paid attention here is that there are oscillations in the frequency responses which does not exist in the previous case with 3SGs in operation. This might be concluded that the oscillations are caused by a poor frequency control support with a low inertial response and primary control. These oscillation needs further investigation about their frequency range and sources which is discussed more detail in the next part.

A three-phase short circuit: A three-phase short-circuit fault occurs for 100 ms at t = 1.6 s and cleared at t = 1.7 s at the bus TRI, and after that, the circuit breaker of TRI load (250 MW) is activated to disconnect the load. In order to support the inertial response, three more SCs are installed in the system at KAS, TRI, and EDR buses that have the same specification with SC3. The locations of SC installation are based on the reactive power support demand through power flow calculation.

The comparative results show that with SCSI not only the frequency stability is improved significantly, but also the system is much more synchronized (Fig. 7). Without any inertia supports of SC and SI, the frequency experiences a huge deviation and ROCOF reaches around 3.5 Hz/s.

A remarkable improvement in the frequency deviation is observed when SIs are in service, the maximum frequency is reduced considerably and rapidly settles down without further increase. On the other hand, a huge enhancement is observed in ROCOF with SC in operation. However, a quite large frequency deviation is witnessed with SC case after the TRI load disconnection. This can be explained that at the first few seconds following the fault, the German side and all of SCs inherently contribute inertial response to the grid by absorbing the power to against the frequency increase that can be observed in a significantly ROCOF improvement. After supporting inertial response, SCs release the energy to the grid to recover their speed which makes the frequency deviation larger compared to the WO case as shown in Fig. 7. This issue is addressed with the combination of SC and SI in operation. ROCOF is drastically enhanced from nearly 3.5 Hz/s (WO) to 2.5 Hz/s that satisfies the acceptable range of the Continental European grid code (±2.5 Hz/s).

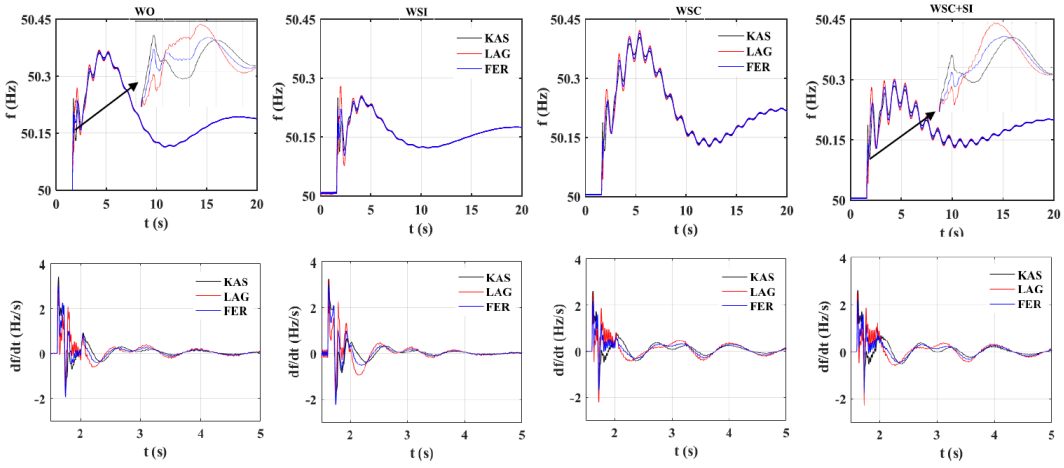

Figure 7. System frequency and ROCOF during a three-phase short-circuit fault with WO, WSI, WSC, and WSC+SI.

1.5.1.4 Conclusion

With a rapid increase of converter-based generation in power system, there is a significant reduction on the system inertia and the primary frequency control. That may cause faster frequency dynamics and a larger frequency deviation during disturbances. Furthermore, the system inertia constant becomes time-variant because of the variability of power dispatch and demand scenarios.

The combination of SC and SI may pronounce the inertial response and a fast frequency control of a synchronous generator during power imbalances. The inertial response from SC remarkably improves ROCOF, afterwards a frequency control support with fast time response from SI of WPPs takes over and significantly enhances frequency deviation. This work is based on the simulation to show how to tune K_{in} and K_{droop} to adjust the output of WPP to support frequency stability and compensate the kinetic energy recovery of SC after its inertial response to help the system quickly settle down. K_{in} is tuned to get a proper power at the beginning of the SI response based on df/dt whereas K_{droop} and T_2 are tuned based on frequency deviation to adjust how large and fast the output of SI is. As a result, a combination of SC and SI provides a better performance that not only enhances frequency deviation and ROCOF but also helps the low inertia system more synchronized during different disturbances.

Operating in low inertia conditions with a poor frequency control support may cause oscillations in frequency response, which makes system quality worse.

1.5.2 Power oscillation damping controller for low inertia systems

The rapid penetration of converter-interfaced generation into power systems renders the system inertia significantly reduced. Low inertia systems with a limit of short-circuit power support from converter-interfaced generation may cause poor dynamic performance and make the system frequency more vulnerable compared to conventional grids. A poor frequency control support in low inertia systems may cause an oscillation (around 0.8 Hz - 1.3 Hz) in frequency responses during disturbances as shown in Figs. 6 and 7.

To address the oscillatory stability issue of traditional power systems, a supplementary controller called power system stabilizer (PSS) is implemented to existing power plants that is used as an auxiliary excitation control to damp generator oscillations. The basic principle of PSS is introducing an electrical torque in phase with the rotor speed variations of power plants to damp the rotor oscillation. This issue is usually solved with small-signal analysis using a linear system model to find the dominant oscillation mode. However, with the dominance of converter-based generators in the modern power systems, new stability issues and requirements for the controls are introduced due to the different physical characteristics and interaction with the grid of converter-interfaced components, traditional PSSs may not work well in the renewable-based systems.

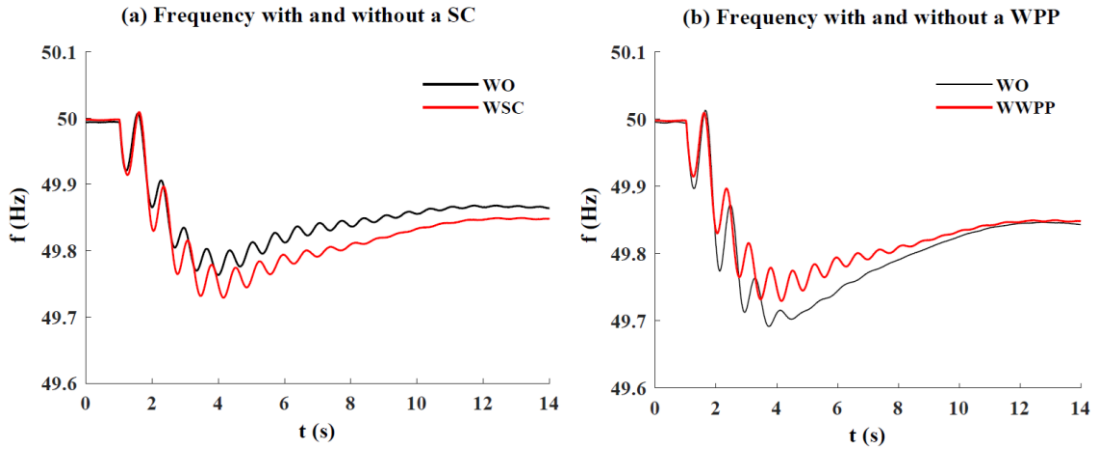

Figure 8.Sensitivities of different components of oscillation in the prospective Western Danish power system. (a) Frequency oscillation without (WO) and with a synchronous condenser (WSC). (b) Frequency oscillation without (WO) and with a major wind power plant (WWPP).

To illustrate the contributions of different components to the oscillation, two scenarios: one applied with/without one major wind power plant and one applied with a synchronous condenser are investigated as shown in Fig. 8. Without a major wind power plant, the post contingency oscillation is highly reduced, while the effect without a synchronous condenser is only a phase delay. It can be envisaged that by having more power converters replacing synchronous machines in the power system, the converters will become the main oscillation source. Due to the complexity of the inertia characteristics of a low inertia system, the mode of oscillation may shift over time, depending on the types of generators online and the design of the converter controls. This requires innovative solutions for oscillation damping controller which adapt to the modern system characteristics to guarantee a secure operation. In this chapter, a power oscillation damping controller incorporating SCs is proposed for low inertia systems which uses a local frequency and a tie line power measurement to control the reactive power of SCs during disturbances. By controlling the terminal voltage through the reactive power of SCs, the active powers of transmission lines, HVDC links, and loads are influenced to damp the oscillation and enhance significantly the frequency stability in terms of frequency nadir and settling time.

1.5.2.1 Power oscillation damping control design

The idea of the control is based on using reactive power to modulate the system voltages, while the change in the voltages will, in turn, affect the active power flow, such as the transmission lines, loads, and HVDC links.

The mathematical formula of the transferred active power on a simplified transmission line can be expressed as:

$$P = \frac{V_1 V_2}{X} \sin \delta$$

where V_1 and V_2 are the line-to-line voltages of the two end sides of the transmission line; δ is the angle of V_1 with respect to V_2; and *X* is the reactance of the transmission line.

The active power of a load expressed in a voltage and frequency dependent load (V&FDL) model is as follows:

$$P_{Load} = P_0(1 + k_{Pf}\Delta f)(p_p + p_c \frac{V}{V_0} + p_z(\frac{V}{V_0})^2)$$

where P_0 is the rated active power of the load; V_0 and V are the nominal and actual voltage magnitude at the load bus, respectively; f_0 and Δf are the nominal frequency and frequency deviation, respectively; k_{Pf} is the frequency characteristic coefficient; and p_p, p_c, and p_c are the portions of total load proportional to constant active power load, constant current load, and constant impedance load, respectively.

The active power of LCC-HVDC link at the rectifier is expressed as follows:

$$P_{HVDC} = 1.654 V_m I_d \cos \alpha$$

where V_m is the peak line-to-line voltage of the AC terminal; I_d is the DC current of the HVDC; and α is the firing angle of the rectifier.

The basic control principle of the LCC-HVDC link is that the rectifier controls the DC current and the α limit, whereas the inverter is responsible for a constant extinction angle control to keep the transferred power tracking to the set point.

From the above equations, the active power on the transmission lines, LCC-HVDC links, and loads can be manipulated by the AC terminal voltage through the reactive power channel. This concept will work under low inertia grids, where the voltage can be affected by the SCs instead of the grid.

A POD control design incorporating SCs adapting to the modern system characteristics is designed in this part. By regulating the terminal voltage through the reactive power modulation, the POD controls the active power transferred on the transmission lines, HVDC links, and loads to damp the power oscillation and improve the frequency stability.

The lead-lag control structure is still preferred due to a better trade-off between the static accuracy, system stability and insensibility to disturbances in the frequency domain. Low-frequency oscillation can be efficiently damped by the proper selection of lead-lag block parameters.

The input of the POD controller is always a point of debate. In the literature, many valuable signals are suggested, including the rotor speed deviation, the frequency, the electrical power or the acceleration power. It is worth noting that the frequency behaviour represents the active power oscillation or imbalance; therefore, it is selected as an input to damp the power oscillation. Furthermore, due to the locality of the frequency in a low inertia system, it is

essential to select a signal from a central path of the oscillation as one of the inputs, where in this case, a measured tie line flow between the Danish and German system is selected. In implementation, this measurement is best taken by synchrophasor measurement units to maintain time synchronization with the local measurements.

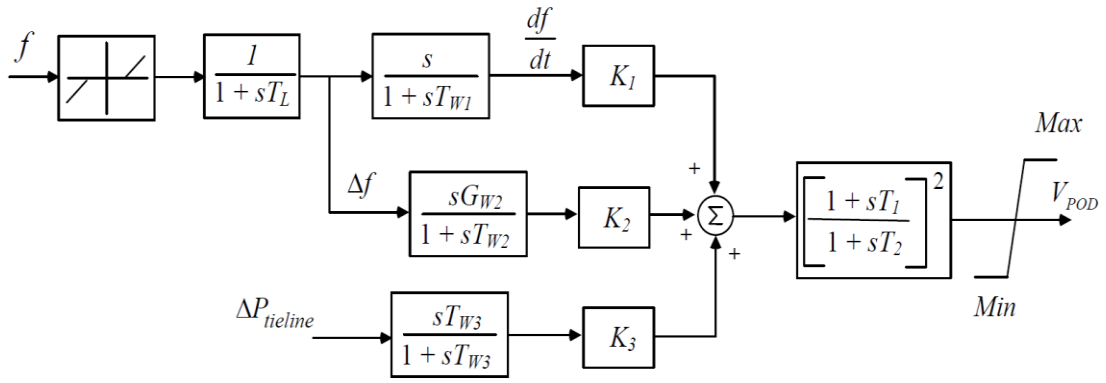

Figure 9. The proposed POD control diagram.

The control diagram of the proposed POD controller is shown in Fig. 9. The local frequency measurement and the active power on a tie line are selected as the input signals of POD to create an output which is added to the AVR of the SC. This output regulates the excitation field current to control the terminal voltage, which therefore changes the active power on the tie line, HVDC links and voltage-dependent loads to enhance the power oscillation and frequency deviation during disturbances. With the frequency input, a deadband is applied to eliminate small frequency changes that may result in an unexpected contribution of POD during steady state conditions. A following low-pass filter $1/(1+sT_L)$ filters the measurement noise that can make the control function poor. There are 2 control signals created by the frequency measurement. The first one, with a small time constant T_{W1}, works like a differentiation to capture the frequency derivation during frequency excursions. The second, with a larger time constant T_{W2}, catches the frequency deviation to generate a signal with a longer response time. The second input (active power on a tie line) first moves through a washout, which allows the desired frequency oscillation mode (inter-area oscillation around 0.1 Hz to 1.5 Hz) to pass and optimizes the compensation at low-frequency range (normally less than 0.5 Hz). Washout time constant is typically adjusted in the range of 2 s - 15 s.

A limiter is a crucial part of each controller that hedges the control participation in conditions of uncertainty. This limiter is more critical when the SC connected to the same bus with voltage-sensitive components, such as PV sources or wind power plants which have strict fault ride-through requirements and voltage-based protection settings. These limitation values may change from site to site depending on grid codes.

The magnitude and phase shift of the output are adjusted through control gains (K_1, K_2, and K_3) and the lead/lag time constants (T_1 and T_2) to compensate the system oscillation. They are optimized by the objective function of genetic algorithms. The GA objective is to maximize the damping ratio of the dominant oscillation mode of the system frequency measurement.

1.5.2.2 POD parameter optimization through software-in-the-loop simulation

Traditionally, to design the PSS or POD control parameters in traditional systems, a linear system model is computed to find the eigenvalues of the system, therefore the dominant oscillation mode is determined. The control parameters are designed based on that dominant mode by increasing its real part, hence moving the mode to the left side of the complex plane.

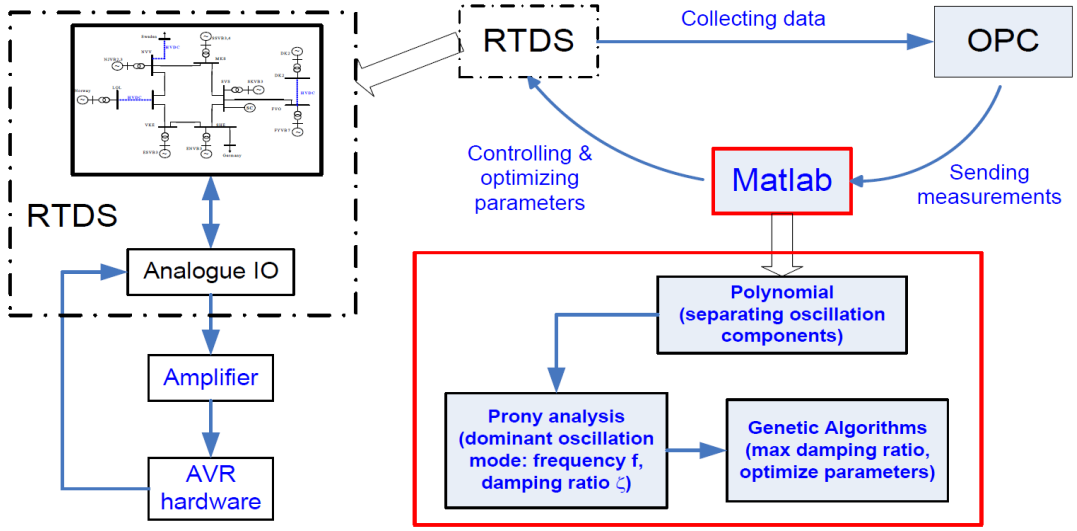

Figure 10. System arrangement of HiL and SiL simulations.

However, in the converter-interfaced systems which are complex and consist of thousands of variables. It is extremely hard to achieve their linear models. As a result, the state-space model may not suit well to these systems. To overcome the issue, Prony technique has been extensively applied based on the measurement data to directly extract the eigenvalues, oscillation frequency, and damping ratio, etc. A nonlinear optimization called GA that is completely independent of the complexity of systems may suit well for parameter optimization of controllers in the modern power systems. With the GA optimization, the issue of parameterization is transformed into a simple optimization problem by setting specific objectives. In this study, a parameter optimization for POD using SiL simulation in real time based on a closed-loop interface among RTDS, Matlab, and OPC is proposed and implemented as shown in Fig. 10. The POD optimal parameter set is determined by the GA objective function that maximizes the damping ratio of the dominant oscillation mode.

The prospective future Western Danish power system run in the RTDS platform is driven by a MATLAB script for system start-up and disturbance simulations. The data of the system are collected by an OPC server and sent directly to the MATLAB workspace. In MATLAB, the signal is first processed to remove the fundamental frequency component. The oscillation component is then analysed by the Prony technique for extracting the frequency and damping ratio of the dominant oscillation mode. The damping ratio is maximized by a GA objective function to determine the better parameters of the POD. After that, these parameters are updated on the RTDS model for further verification. These steps are iterative by a closed-loop and run in real time with the RTDS, OPC, and MATLAB communications as shown in Fig. 10. The loop will continue until the objective function satisfies the damping ratio maximization of the dominant mode constraint to determine the optimal values of POD parameters.

1.5.2.3 Prony analysis

A Prony analysis is a least-square approximation technique of fitting a linear sum of exponential terms to a measured signal. The important feature of this technique is that it directly determines the frequency, damping ratio, energy, and relative phase of the modal components present in a given measurement signal by an extended Fourier analysis. The ability to extract such information from transient signal simulations would overcome the computing burden of the linear model for large-scale systems, which consists of thousands of variables.

Consider a generally continuous signal $\hat{y}(n)$ that is to be modelled by

$$\hat{y}(n) = \sum_{i=1}^{p} (b_i z_i^n) = \sum_{i=1}^{p} A_i e^{j\theta_i} e^{(\alpha_i + j2\pi f_i)n\Delta t}$$

with

$$\begin{cases} b_i = A_i e^{j\theta_i} \\ z_i = e^{(\alpha_i + j2\pi f_i)n\Delta t} \end{cases}$$

where n=0, 1, 2, ..., N-1, N is the sampling number; Δt is the time interval of sampling; p is the order of the Prony mode; A_i and θ_i are the amplitude and inception phase angle of the i-th oscillation mode, respectively; and f_i and θ_i are the frequency and damping ratio of the i-th oscillation mode, respectively.

Overall, the Prony analysis can be summarized into three steps:
1. Constructing a linear prediction model from the measured data and solving it.
2. Computing the discrete-time poles of the characteristic polynomial equation generated by the linear model which in turn results in the eigenvalues.
3. From these eigenvalues, the damping ratios and oscillation frequencies and related parameters can be extracted.

A polynomial fitting is implemented to find the fundamental frequency component. This step separates the oscillatory component for Prony analysis conduction. The Prony analysis obtains many oscillation modes which include the dominant mode and disturbance modes. This results from the mixing noise and trend in the measurement which cannot be eliminated completely in the signal processing step.

The dominant mode is recognized by the energy analysis approach, which evaluates the contribution of each oscillation mode and is expressed as follows:

$$E_i = \sum_{n=0}^{N-1} (R_i z_i^n)^2$$

Where E_i, R_i, and z_i are the energy, the amplitude, and the pole of the i-th oscillation mode, respectively; i=1, 2, ..., p.
The entire oscillation energy is defined as follows:

$$E_{tot} = \sum_{n=0}^{N-1} \left[\hat{y}(n)\right]^2$$

Then the contribution of the i-th oscillation mode can be expressed as:

$$\eta_i = \frac{E_i}{E_{tot}}$$

The dominant mode is determined by the largest energy contribution to the oscillation.

1.5.2.4 Genetic algorithm

An optimization approach is a mathematical model where the main objective function is to minimize undesirable things (e.g., costs, errors, and losses) or maximize desirable things (e.g., efficiency, damping ratio, and profit), subject to constraints. Two main approaches exist for the optimization problem: linear and nonlinear methods. The linear approach is based on the linear system model using small-signal analysis, which depends on the initial operation point with several simplifications, e.g., does not consider discrete control behaviours, such as limiters and saturation. As a result, when a control system reaches its limiters during disturbances may be inaccurate. Conversely, the nonlinear method is usually applied to the simulation-based approach, which is less restricted by modelling limitations.

The evaluated system is simulated in real time in RTDS using an electromagnetic transient (EMT) model that employs large-signal analysis and is more accurate than the RMS model using small-signal analysis. Due to this study, which employs the simulation-based approach, a nonlinear optimization tool that is referred to as a genetic algorithm is applied to optimize the controller parameters.

A GA is a global heuristics parameter search technique that is based on genetic operators to find the optimal or near-optimal solutions for a specific problem. Unlike the traditional optimization approaches that require one starting point, a GA uses a set of points (chromosomes) as the initial condition, and the performance of each chromosome is evaluated according to the objective function that characterizes the problem to be solved and defined by the designers. A group of chromosomes is referred to as a population. The process of GA is applied as follows:

1. Initialization: a number of individuals represent the POD parameters that are randomly created according to the initial population, upper and lower bound setting.
2. Objective evaluation: Using a selection operator, the algorithms select the best result for each individual in accordance with their values defined by the objective function. The main goal of the control system is maximizing the damping ratio of the system oscillation mode, i.e.,

$$f(x) = max\left\{ \xi = -\frac{\alpha}{\sqrt{\alpha^2 + \beta^2}} \right\}$$

1. subject to

$$T_{imin} \le T_i \le T_{imax} \, (i = 1,2)$$

$$K_{jmin} \le K_j \le K_{jmax} \, (j = 1,2,3)$$

2. where α and β are the real and imaginary parts of the dominant mode, respectively. This equation means that GA determines the variables x (T_1 , T_2 , K_1 , K_2 , and K_3) based on the boundary settings to maximize the damping ratio ξ of the oscillation mode.
3. Reproduction: a new set of chromosomes are generated from the selected parameters in step 2 using selection, crossover, and mutation operators. These genetic operators ensure a larger average objective value for next generations.
4. Termination flagged: these 3 steps are repeated continuously until one of the termination parameters is achieved. The GA may be terminated after a certain number of generations when the objective value does not enhance after a certain generation. The whole procedure of parameterization for POD base on a SiL is shown in Fig. 11.

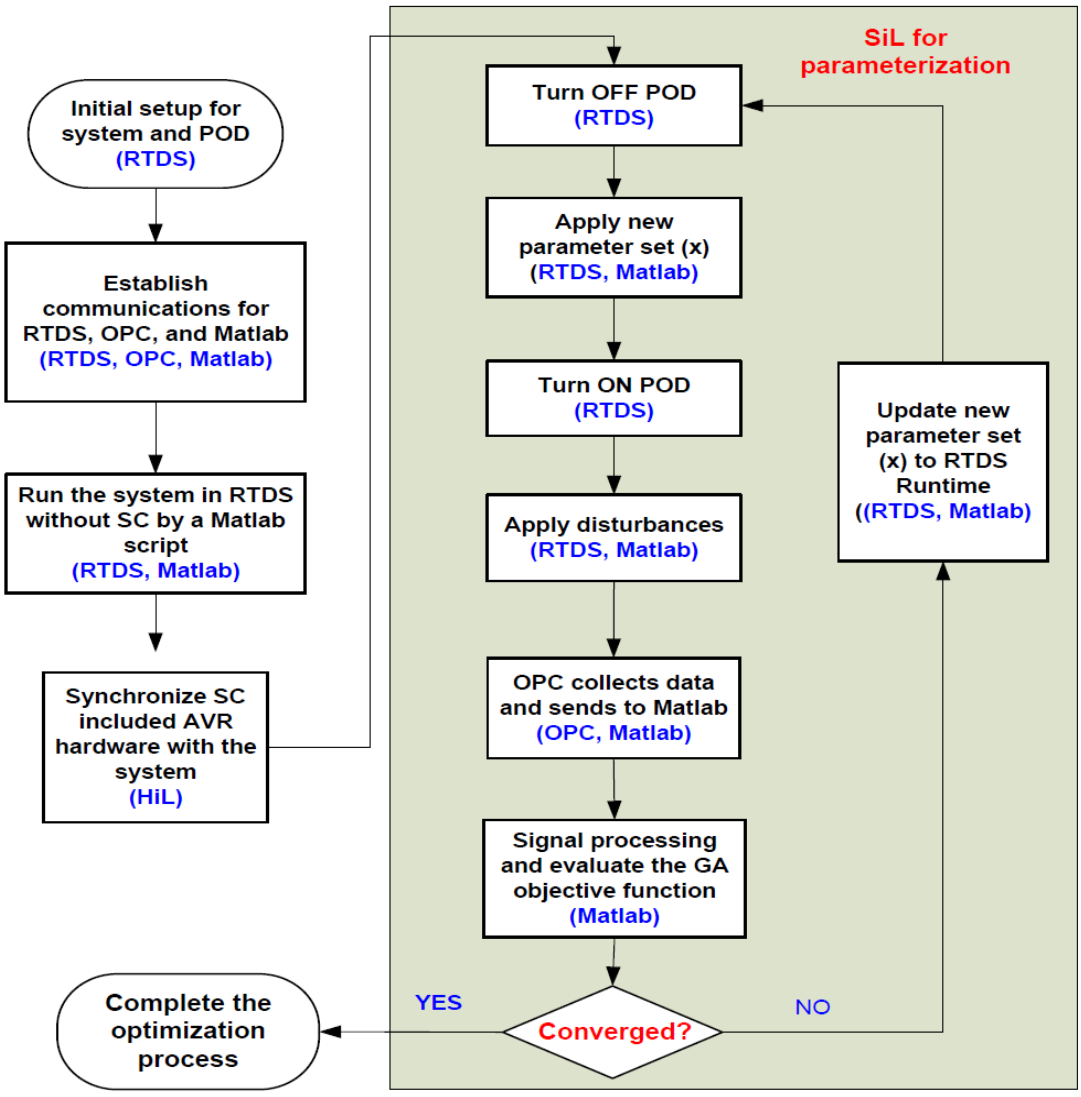

Figure 11. The flowchart of parameterization process of POD.

1.5.2.5 Case study

To verify the performance of the proposed method on the damping and frequency stability, a load increase disturbance and a three-phase short-circuit fault are investigated in this section. To determine how the PSS performs in low inertia systems, a comparison of system responses with PSS, with GA-based POD and without either is investigated in the first scenario. It is worth noting that the modelled future Danish power system is a typical low inertia system due to a high installation of RE, HVDC links, and a weaker German grid. The Danish electricity system is divided into two nonsynchronous areas: The Western Danish power system (DK1) is synchronized with the continental European system, whereas the Eastern Danish power system (DK2) is synchronized with the Nordic power system that also includes Sweden, Norway, and Finland. DK1 and DK2 are linked by an LCC-HVDC interconnection. This connection is known as the Great Belt Power Link, which has a 400 kV DC connection with a transmission capacity of 600 MW. The single-line diagram of a 400 kV DK1 renewable-based system in 2020 is shown in Fig. 12 and is used for the case study system in this work. In this study, all synchronous generators are phased out and there are six synchronous condensers installed in the system, while the SCs at FGD and KAS (SC3 and SC4) are equipped with the proposed POD controller.

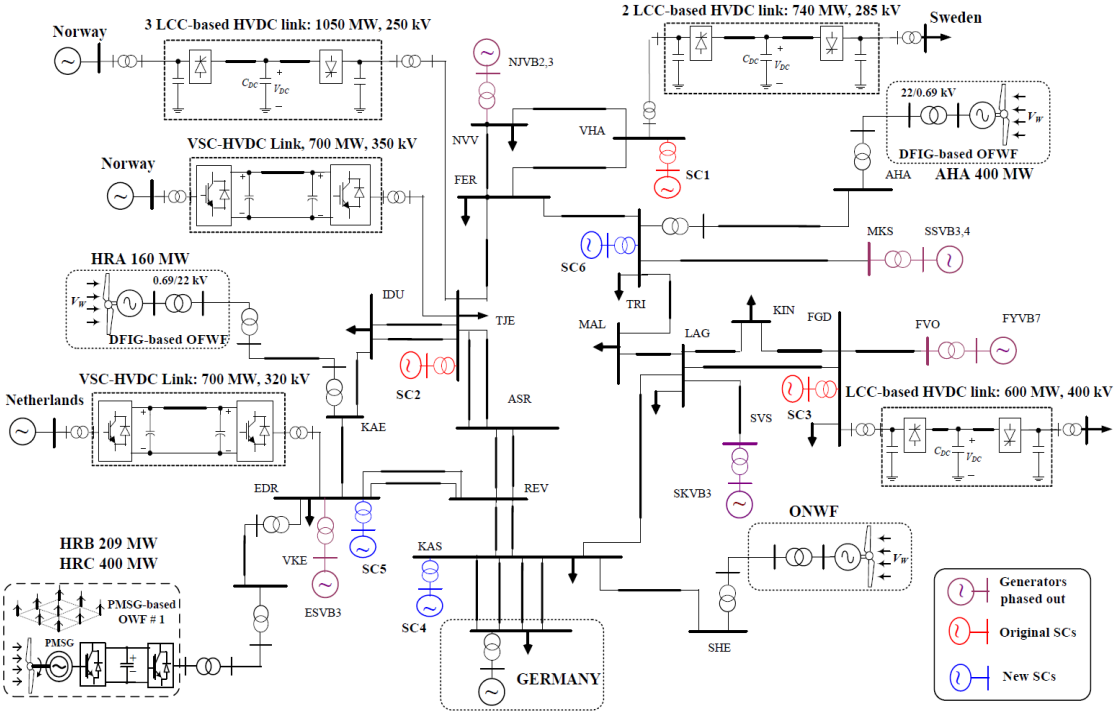

Figure 12. Single-line diagram of a 400 kV Western Danish renewable-based system in 2020.

1) Load increase disturbance

A comparison of the system responses with PSS (PSS), with GA-based POD (GA-POD), and without either (WO) during a load increase disturbance is intuitively shown in this scenario. Fig. 13 shows the comparative results of the system frequency, ROCOF, active power on transmission line KAS to LAG, LCC-HVDC, VSC-HVDC links, load, and the SC responses. The responses are without in the dotted black lines, with the PSS in the dash and dotted red lines, and with the GA-based POD in the solid blue lines, respectively. From the comparative results, it can clearly be seen that with the POD controller, the system response is signifi-

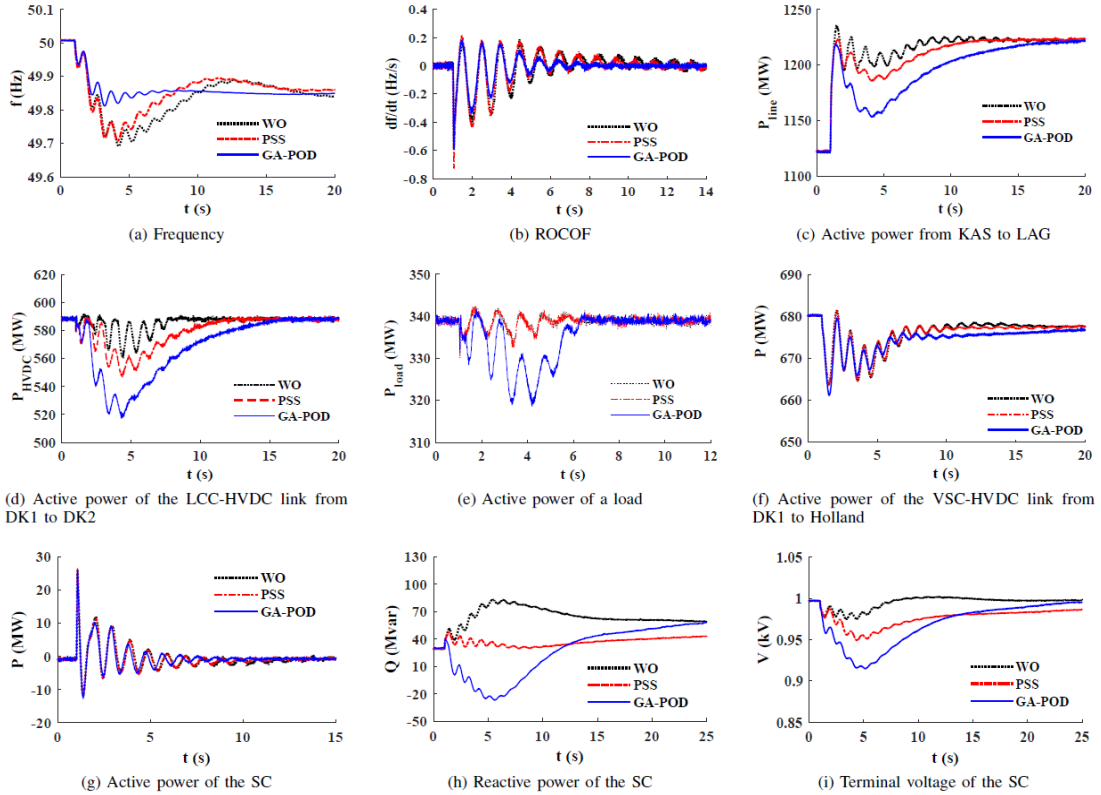

(a) Frequency (b) ROCOF (c) Active power from KAS to LAG

(d) Active power of the LCC-HVDC link from DK1 to DK2 (e) Active power of a load (f) Active power of the VSC-HVDC link from DK1 to Holland

(g) Active power of the SC (h) Reactive power of the SC (i) Terminal voltage of the SC

Figure 13. Load increase scenario.

cantly enhanced in terms of the damping ratio and frequency stability. By comparing the system frequency in Fig. 13(a), without the POD it experiences a large and long oscillation (the dominant mode has a 0.079 damping ratio) as well as a significant frequency deviation (0.3 Hz) before obtaining a new equilibrium. In contrast, with the GA-based POD these parameters are remarkably improved by a damping ratio of 0.29 and a frequency deviation of 0.18 Hz. The frequency rapidly reaches the steady-state condition. Taking a look at the ROCOF, faster damping and quicker settling down are obviously seen in Fig. 13(b) with the POD controller.

The active powers on the transmission line from KAS to LAG, HVDC links, and load are controlled during the disturbance to reduce the power imbalance and damp the oscillation. As a result, the system frequency with the GA-based POD is improved in terms of the oscillation damping, frequency nadir, and settling time, as shown in Fig. 13.

An opposite trend is observed from the reactive power response of the SC during the disturbance without and with the POD controller as shown in Fig. 13(h). Instead of rapidly increasing the reactive power from 31 Mvar to approximately 83 Mvar to keep the voltage constant at the nominal value as in the WO case, the POD decreases the terminal voltage by absorbing approximately 58 Mvar reactive power (from 31 Mvar to approximately -27 Mvar) to control the power flow. Consequently, a large decrease and less oscillation are seen from the active powers on the transmission lines, HVDC links, and load with the POD controller as shown in Fig. 13.

As expected, the SC rapidly releases kinetic energy for the inertial response and quickly settles down with the POD controller as seen in Fig. 13. As a result, the power oscillation damping and frequency stability are improved during the disturbance with the POD controller. The comparison of the dominant mode information with PSS, with POD, and without either is listed in Table 1, which shows a significant enhancement in terms of the frequency stability and power damping with the POD controller. The settling time and frequency nadir are improved significantly from 17 s and 49.7 Hz to 8 s and 49.82 Hz without and with the GA-based POD, respectively.

To clarify the active power decrease of the LCC-HVDC link, the rectifier is set to maintain the DC current at its set-point by controlling the firing angle. When the busbar voltage decreases, the DC current is less than its order, and the rectifier tends to reduce the firing angle, hence increasing the DC current. However, the firing angle reduction hits the minimum firing angle limit (typical 5^0). This results in the DC current decreasing, thereby reducing the HVDC active power during the disturbance.

By comparison, the PSS does not handle well in the converter-based system, while the GA-based POD can further improve the frequency stability and damping ratio by absorbing more reactive power to allow for a lower voltage but still satisfy the grid code.

Table 1. Without, with PSS, and with GA-based POD comparison of dominant mode.

Cases	*Dominant mode*	*Frequency (Hz)*	*Damping ratio*	*Frequency nadir (Hz)*	*Settling time (s)*
WO	-0.525±*j*6.585	1.048	0.079	49.7	~ 17
WPSS	-0.635±*j*6.870	1.093	0.092	49.71	~ 16
WPOD	-1.933±*j*6.379	1.015	0.29	49.82	~ 8

2) Three-phase short-circuit fault

The POD controller is verified through a severe disturbance with a three-phase short-circuit fault and a load trip occurring simultaneously. At t = 1 s, a three-phase short-circuit fault is applied on one of the feeders of the TRI bus and cleared at t = 1.1 s, then the circuit breaker of the feeder suddenly disconnects the load (250 MW). Figs. 14 and 15 show the comparison of the system responses without and with the GA-based POD controller. A similar pattern is

plotted in this scenario. While the uncontrolled system exhibits a severe oscillation and system collapse after approximately 4 s, the system with the POD controller performs a better damping and becomes stable after the fault.

As shown in Fig. 16, for the scenario without the POD (WO), after the fault the frequencies at different substations tend to oscillate against each other, which leads to a system collapse, while they quickly become stable with the GA-based POD (GA). Because of the asynchronism issue, the active power could not transfer from Germany to the DK2 system through the transmission line KAS to LAG, HVDC link, and load as shown in Figs. 14 and 15.

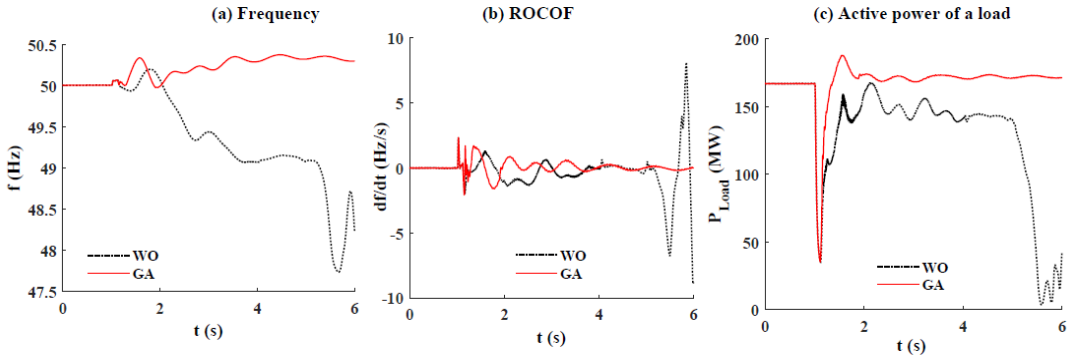

Figure 15. Three-phase short-circuit fault scenario. (a) System frequency. (b) ROCOF. (c) Active power of the FER load.

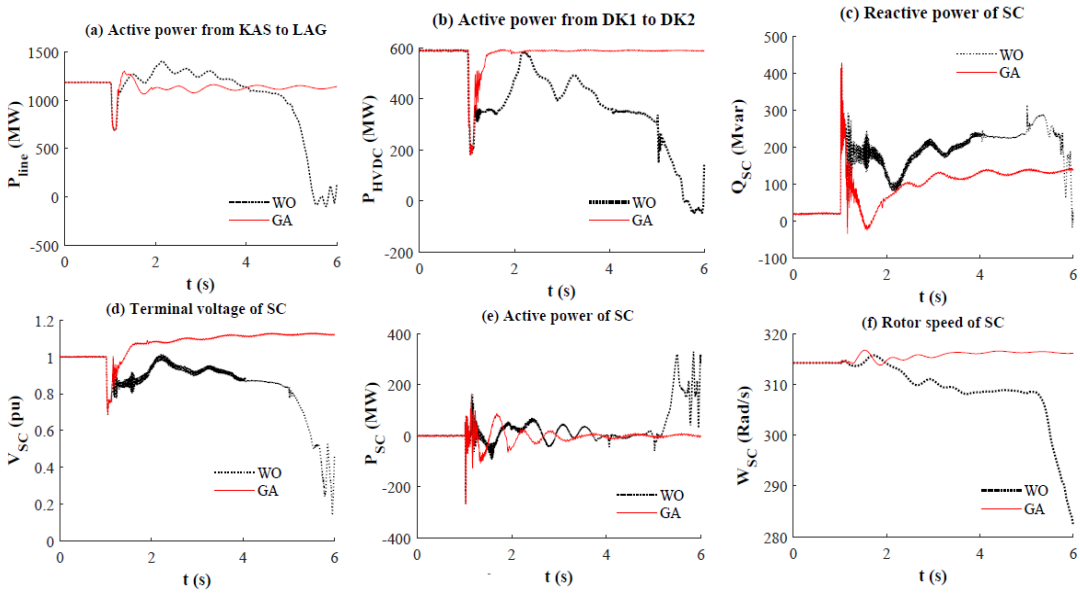

Figure 14. Three-phase short-circuit fault scenario. (a) Active power from KAS to LAG. (b) Active power from DK1 to DK2 through HVDC connection. (c) Reactive power of the SC. (d) Terminal voltage of the SC. (e) Active power of the SC. (f) Rotor speed of the SC.

Instead of decreasing the reactive power to prevent the voltage surge, the POD allows terminal voltage to increase within the limit range. Therefore, the transmission line, HVDC link, and load can absorb more active power to offset the power imbalance during the load trip, as can be intuitively seen in Fig. 14 and Fig. 15. This phenomenon helps the system maintaining stability after the fault.

In this scenario, the active power of the HVDC link does not significantly contribute to the power oscillation control during the disturbance with the GA-based POD. It can be explained that the busbar voltage increases, making the DC current higher than the current set-point. With the ability of firing angle control to transiently reach 90^0 in order to quickly reduce the DC current, the active power can be kept constant during the voltage increase. In contrast,

the load tends to absorb more active power to counteract the power imbalance and damp the oscillation, as seen in Fig. 14.

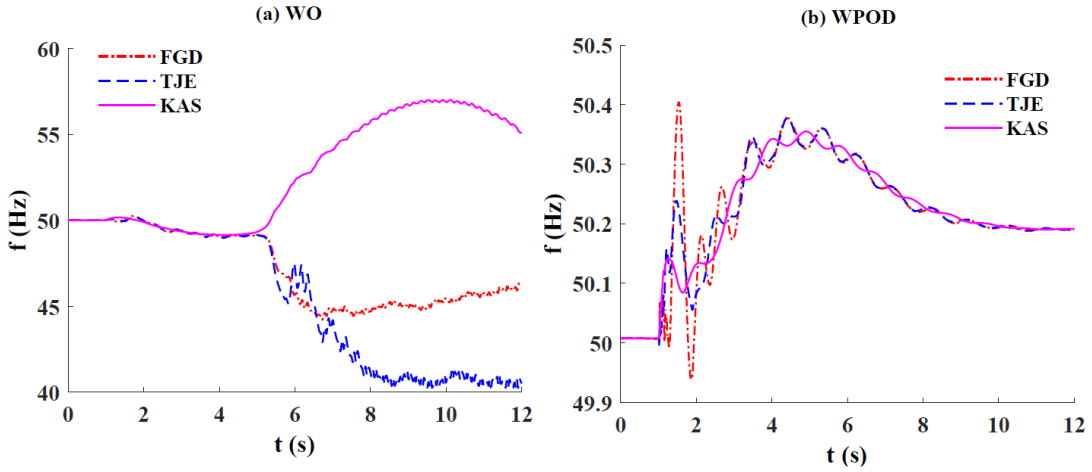

Figure 16. Frequency responses at different substations during a three-phase short-circuit fault. (a) WO. (b) WPOD.

1.5.2.6 Conclusion

The dominance of converter-based generation in modern power systems causes system inertia significantly reduced, which may create more challenges for system frequency stability and control. Additionally, new stability issues and requirements for the controls are introduced due to the different physical characteristics and interaction with the grid of converter-interfaced components. Consequently, faster frequency dynamics with a higher rate of change of frequency and a larger frequency deviation during disturbances resulted as its certain consequences. Furthermore, the system inertia constant becomes time-variant due to the variability of power dispatch and demand scenarios. A poor frequency response may cause oscillatory issues in frequency responses during disturbances, which worsens the system situation.

To deal with the oscillatory stability issue for converter-based systems where new stability issues and requirements for the controls are introduced, the ability of SCs for providing a power oscillation damping with a proper control approach named POD has been proposed. The control uses the local frequency measurement and the active power on a tie line to control the reactive power of SC. Consequently, the voltage at the SC-connected busbar is controlled, which in turn manipulates the active power flow on transmission lines, load, and HVDC links to damp power oscillation. The parameter is optimized based on a SiL simulation using Prony analysis from the simulation results and a nonlinear optimization tool that is suitable for large-scale power systems with thousands of state variables.

Application of this controller is simple for existing SCs on the grid to provide the supplementary control service for frequency control and oscillation damping. To properly apply the POD controller to a specific grid, the following important discussion is presented:

1. Controlling the terminal voltage of SC to change the active power should consider the limitation of the transmission lines, HVDC links, and loads to establish the limit values for the POD output.
2. The limits of the terminal voltage of the connected busbar may impact the components connected to the same bus of the SC (PV system, wind generator), which are sensitive to the low-voltage ride-through threshold and voltage-based protection.
3. The line flow selected as the control input should represent the power oscillation where the dominant power exchange occurs.

1.5.3 Assesment of short circuit power and protection systems

1.5.3.1 Short circuit power characterization

Fault studies are an crucial part of power system analysis. Power system faults can be generally classified into three-phase balanced faults, and unbalanced faults which consist of single line-toground fault, line-to-line fault, and double line-to-groud fault. The characteristics of the short circuit current mainly depend on the network configuration and the impedance of its components through which the short circuit current passes. In a conventional power system, SGs are the main sources of the short circuit current and the characteristics of the short circuit current can be illustrated by Fig. 17. The short circuit impedance of an SG under short circuit conditions is a time-varying quantity. For the purpose of fault studies, the corresponding short circuit current is typically classified into the subtransient period (the first few cycles), transient period (the next a few cycles), and steady-state period. As synchronous machines, synchrous condensers have similar short circuit response as synchrous generators in terms of magnitudes and phase relationships in faulty phases. During the fault, both SG and SC naturally contribute a considerate amount of reactive power. The SC cannot provide sustaining active power but as a rotating machine, the SC provides inertia response resulting in its active power exchange with the grid. Figure 18 shows an example comparing the short circuit response of an SG and a SC subject to A-B fault at the machine terminal.

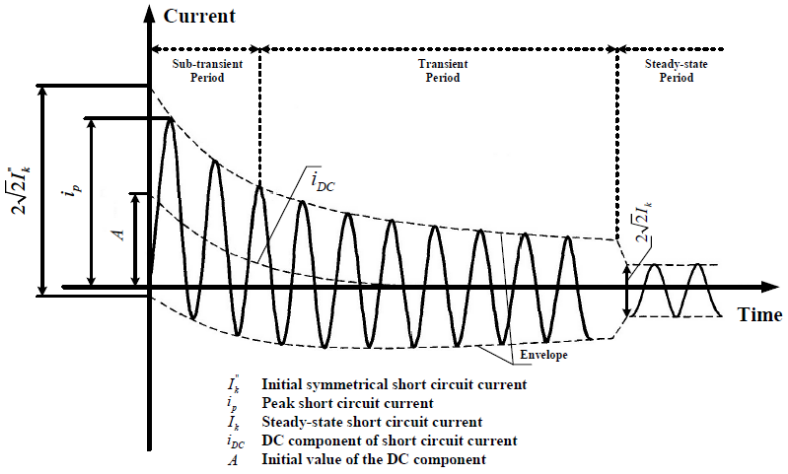

Figure 17. Schematic diagram of the short circuit current of a near-to-generator short circuit withdecaying AC component

However, the short circuit response of voltage source converters can be significantly different from that of synchronous machines. It is mainly decided by the hardware limits and the design of the control systems. Typically, for a current-controlled VSC system, the control system shown in Fig. 19 consists of a slower outer controller and a faster inner current controller. The outer controller regulates the DC side voltage, the AC side voltage, and the output powers at the PCC depending on the application. It generates current references for the inner current controller that regulates the converter current.

The control system shown in Fig. 20 is typically used for a grid connected VSC. Corresponding to a three-phase balanced fault at the PCC in Fig. 19, Fig. 21(a) presents the short circuit response of the VSC when there is no converter current peak limit imposed. The VSC provides a set of balanced short circuit current during the fault. The active power remains the same as the pre-fault level and the reactive power increases to a certain level after some initial transients. The short circuit response with a 1.2 p.u. converter peak current limit is given in Fig. 21(b), where the reactive current injection is prioritized. The actual active current refernece is decided by how much current margin is left after satisfying the reactive current injection. As a result, the active power from the VSC is curtailed during the fault to comply with the current limit. By comparing Fig. 21 with Fig. 17, it can be observed that the

short circuit current from the VSC is restricted in the magnitude and its characteristic does not comply with the schematic diagram in Fig. 17 for synchronous sources.

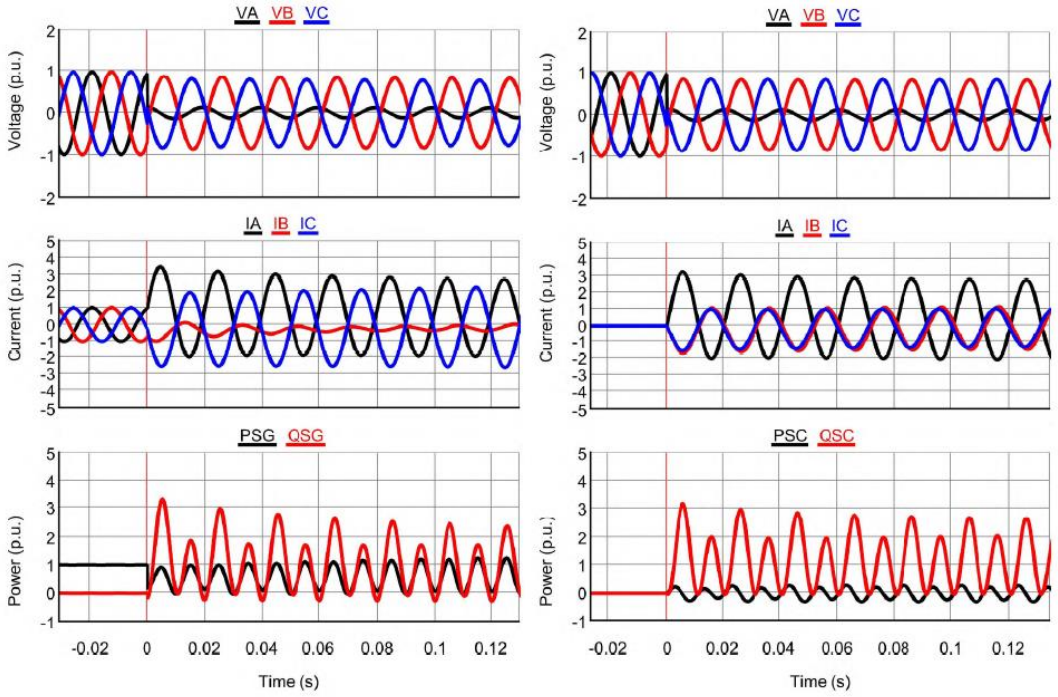

Figure 18. Short circuit response of an SG (left) and an SC (right) under A-B fault

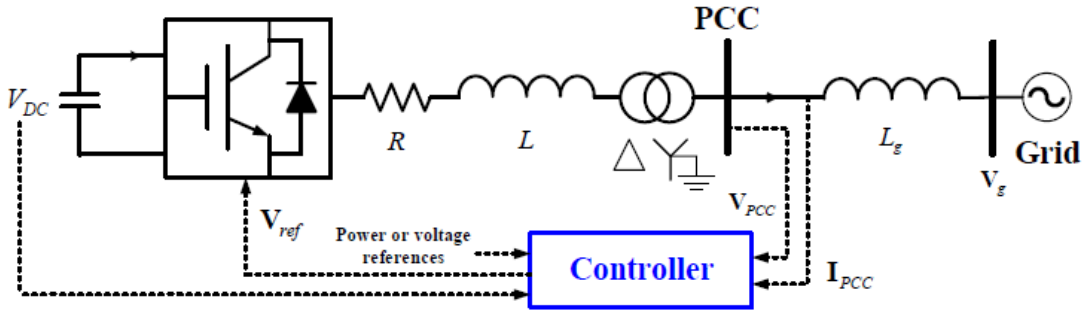

Figure 19. Configuration of a grid-connected VSC system.

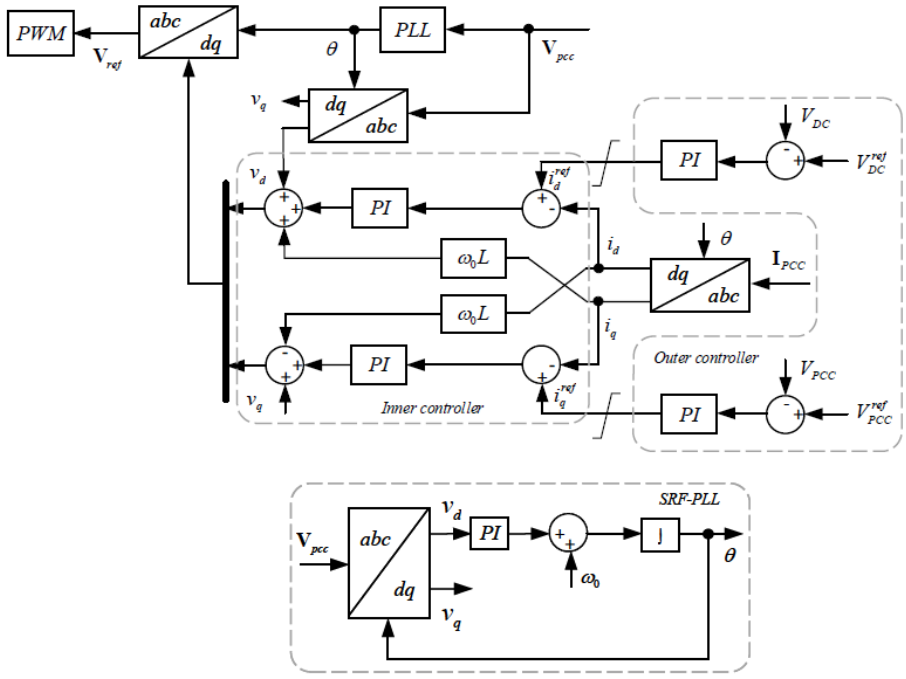

Figure 20. Control block diagram of a grid-connected VSC in synchronous reference frame.

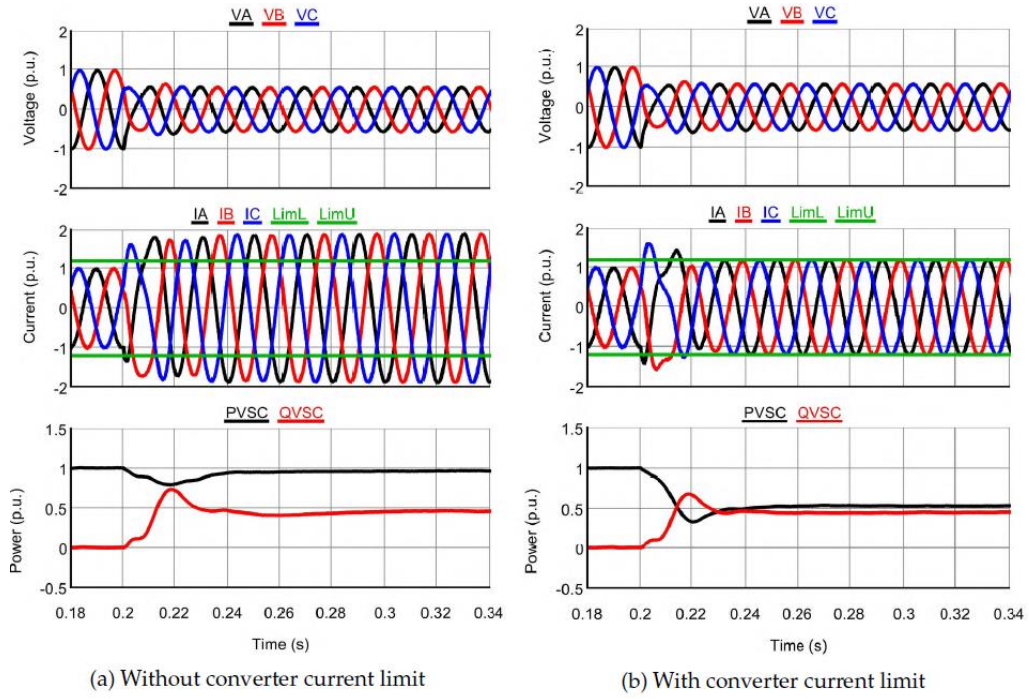

Figure 21. Short circuit response of a VSC under three-phase balanced faults

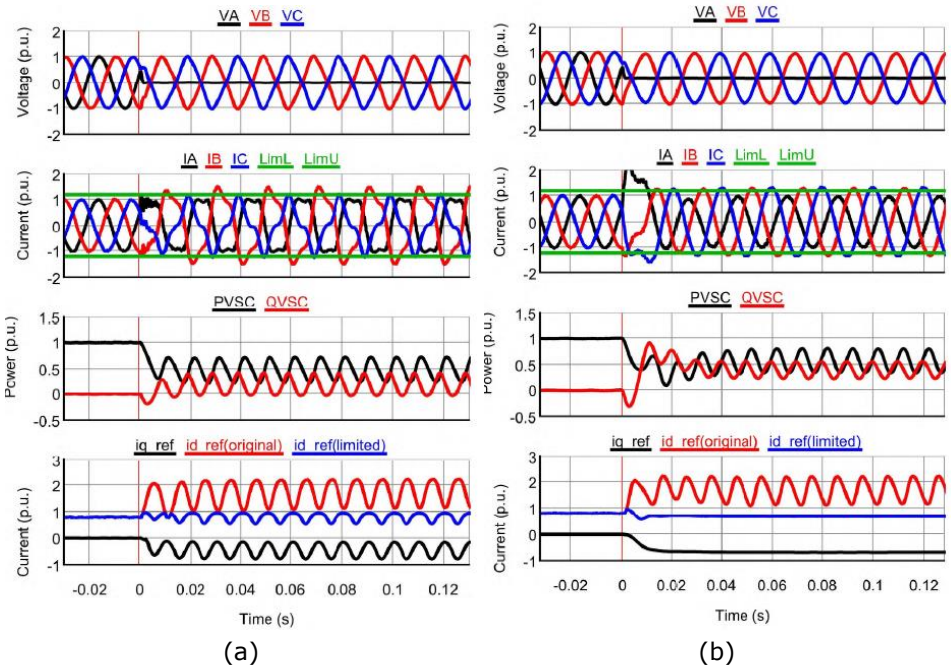

Figure 22. Short circuit response of a VSC under A-B fault

However, the control system show in Fig. 20 does not perform in unbalanced faults due to the existence of negative-sequence scenarios. As an example, Fig. 22(a) shows the response of the VSC under A-B fault at the PCC. This is because that the park transformation of a set of unbalanced three-phase signals will introduce AC terms in superpositions with DC terms, but PI controller is designed for regulating DC signals. As a result, the control system in Fig. 20 is contaminated with AC terms and the generated modulation waves for the PWM become non-sinusoidal. Then, the controller is modified by using only the positive-sequence voltage and current as inputs. The current references are filtered by notch filters to eliminate the AC terms. The corresponding VSC short circuit response is given in Fig. 22(b). For the same fault conditions, the voltage and current are free of distortions and exhibit sinusoidal waveforms. However, the converter peak current is still not within the pre-defined limit after the initial transients. The reason is that the controller in Fig. 20 is only implemented in the SRF for the positive-sequence component, leaving the negative-sequence current unregulated.

This indicates that, the negative-sequence current from the VSC should be controlled properly.

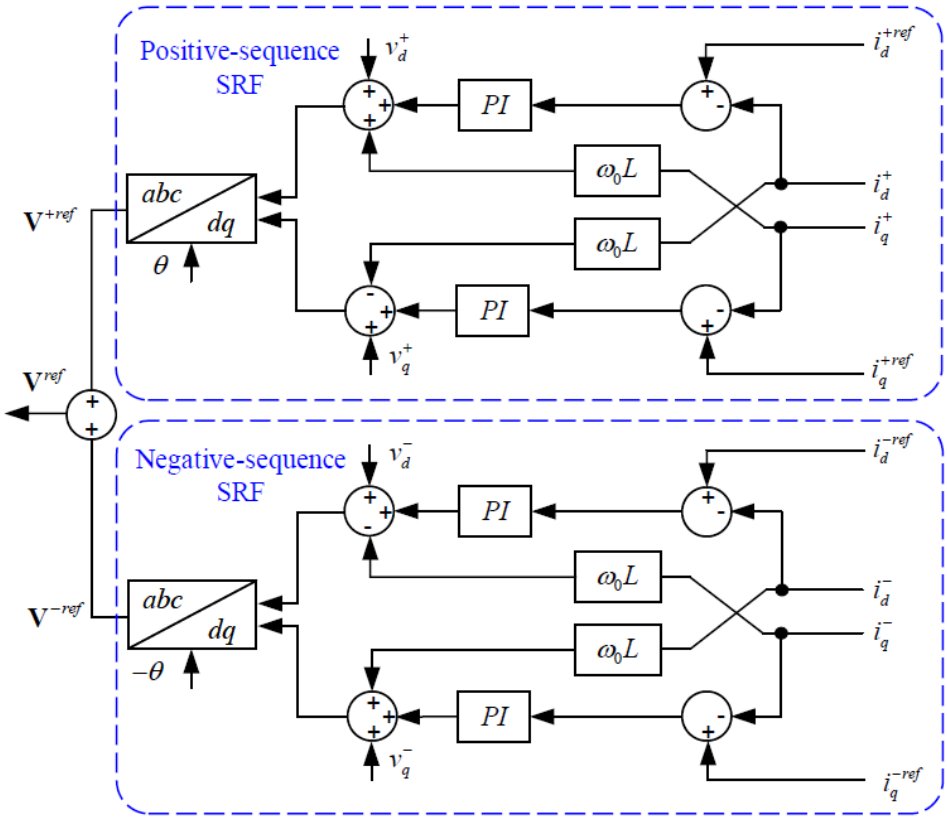

Figure 23. Inner current controller of a grid-connected VSC with dual-sequence current control

Figure 23 shows the control block diagram of a dual-sequence current controller. This method applies two sets of PI controllers, one regulating only positive-sequence current in postivesequence, and the other regulating only negative-sequence current in negative-sequence. This allows the current in diffeerent sequences to be controlled as DC signals. Then the question left is how the current reference should be generated. In the literature, there exist a variety ways of generating current references in dual-sequence. However, there lacks a general way of characterzing the short circuit current from VSCs considering simultaneous injection of active and reactive power, and condisering the current limit in each single phase. This work package proposed an unified manner to represent the control strategies based on instantaneous power theory and voltage support concept. One group of control strategies is named as: Flexible Oscillating Power Control (FOPC). The idea is that by introducing flexible parameters in the current references, the short circuit response can be freely adjusted. As shown in Fig. 24, the amplitudes of the power oscillations during the fault are gradually changing with with different parameters. The second grounp of control strategies is named as: Flexible Positive- and Negative-Sequence Power Control (FPNSPC). By choosing different values of the flexible parameters, the relative amount between the positive- and negative-sequence powers during the fault can be freely adjusted. As an example, Fig. 25 shows the variation of short circuit response of a VSC during A-B fault with FPNSPC, where the relative amount of positive-sequence reactive power and negative-sequence reactive power is flexibly adjusted with different values of the control parameters.

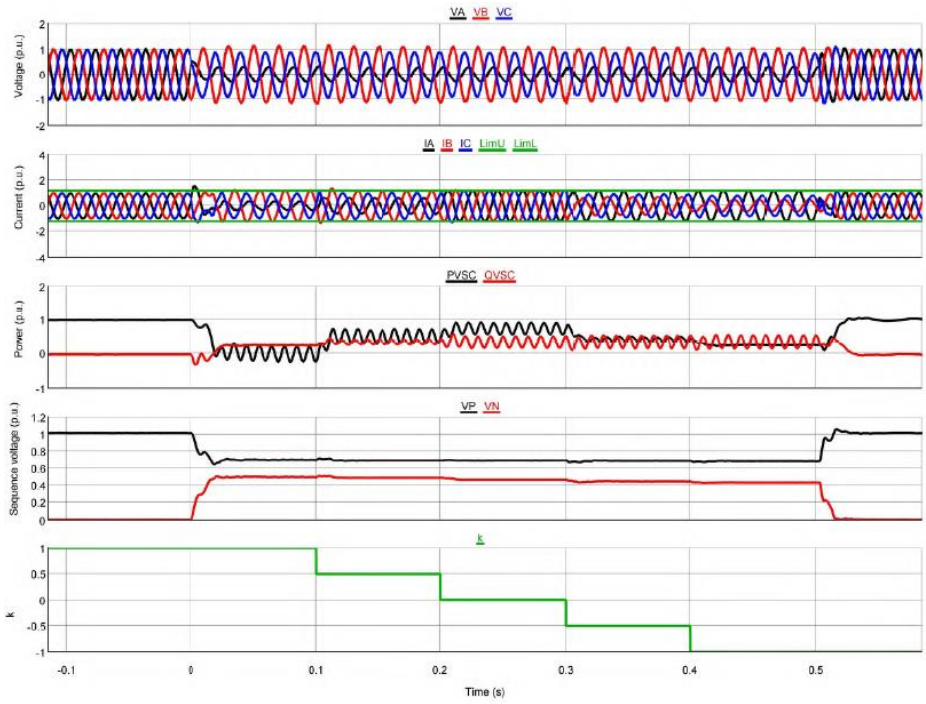

Figure 24. Short circuit response of a VSC under A-g fault with FOPC

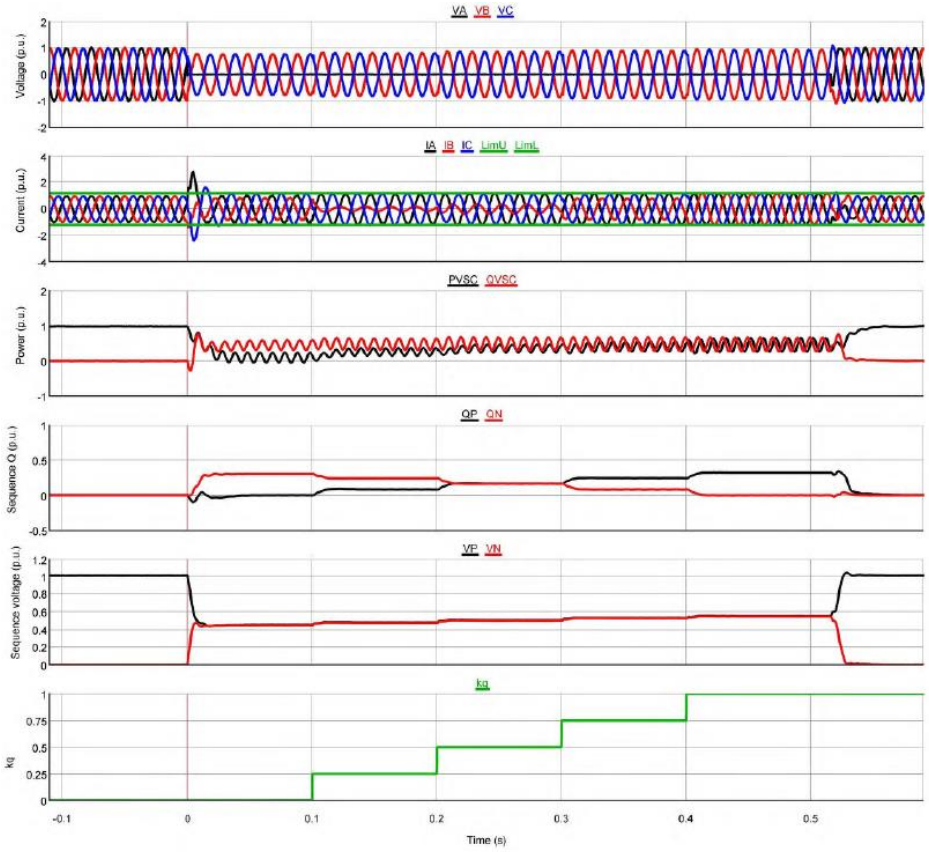

Figure 25. Short circuit response of a VSC under A-B fault with FPNSPC

The current flowing through converters should be restricted in each individual phase due to the limited semiconductor overload capability. For a three-phase balanced fault, the short circuit current from a VSC does not contain any negative-sequence component ideally. This makes the design of converter peak current limit straightforward. However, the converter peak current limit method becomes more complicated if negative-sequence current is injected under unbalanced faults. This is because the superposition of positive- and negative-sequence current will boost the current in a certain phase and it is depending on different conditions such as fault type, control strategies, grid configuration, etc. This work developed

generic converter current limit as shown in Fig. 26. In this way, the converter current is restricted through the maximum allowable power injection, and it is valid for all kinds of control strategies as indicated in Figs. 24-25.

It can be seen from Figs. 24-25 that the short circuit response of VSCs under unbalanced faults can be significantly different from each other and from synchronous souces. However, the different controls strategies can be further unified as indicated in Fig. 27. If a coordinate is used to represent the selection on flexible control parameters in FPNSPC and FOPC as shown in Fig. 27(a) and 27(b) respectively, the black line in Fig. 27(b) can be translated into the blue line in Fig. 27(c). This means that as long as the kp-kq joint strategy is determined in one group of the flexible control strategies, the kp-kq relationship is also determined in the other group so that they are equivalent to each other. Therefore, the short circuit power from VSCs with different dual-sequence current control strategies can be characterized by the different combinations of the sequence powers (P+, P−, Q+ and Q−).

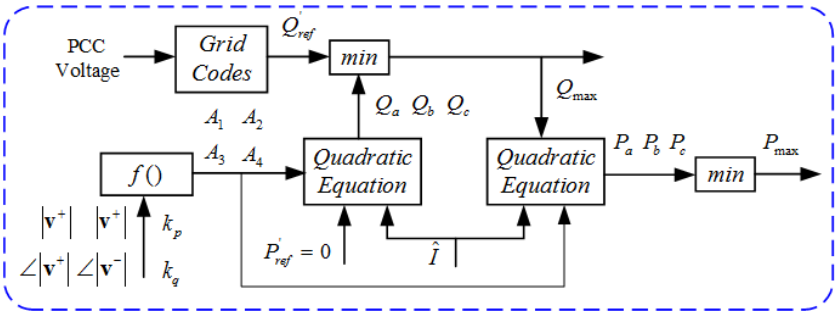

Figure 26. Schematic diagram of the converter current limiter

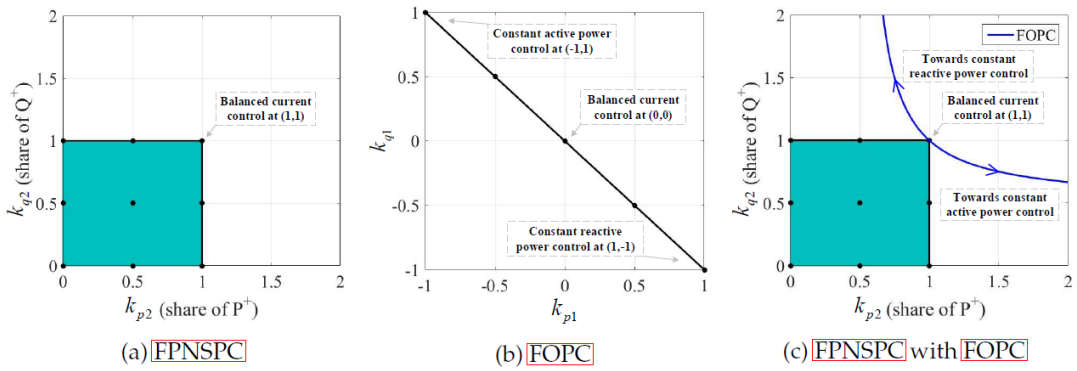

Figure 27. Relationship between FOPC and FPNSPC.

1.5.3.2 Combined effect of VSC and SC

Synchronous condensers have the advantages of contributing short circuit current, enhancing system frequency stability and providing voltage support. It has been shown in the literature that there is a need of more SCs for a future low inertia power system. Even though the conventional power plants can be reimbursed into SCs, their locations may not be the optimal ones and newly-installed SCs can be anticipated at the PCC of a HVDC system or a wind power plant. Therefore, it is necessary to examine the combined effect of VSC and SC taking

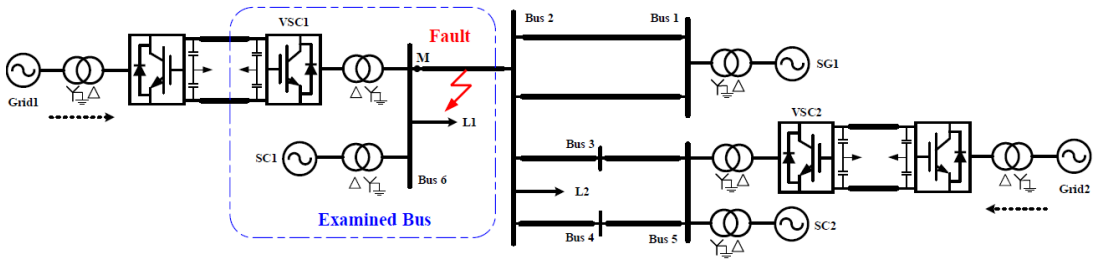

Figure 28. Single-line digram of the studied system with SCs

VSC control strategies into consideration. Here, the combined effect is investigated in terms of four aspects: short circuit current, PCC voltage, DC-side voltage and frequency response during faults.

The system shown Fig. 28 is used for investigation, and the focus in given to Bus 6 where there is a VSC-HVDC converter and a synchronous condenser. The control strategy of VSC1 and the capacity of SC1 can be varied as different scenarios. Firstly, the phases of the short circuit current from VSC and SC can be significantly different. As a result, there can potentially exist current cancellation problem. As an example in Fig. 29, with VSC using constant active power control strategy, the application of synchronous condenser helps increase the fault current level. The larger the capacity of SC, the higher the fault current. In contrast, with constant reactive power control strategy, the application of a 50 Mvar synchronous condenser even reduce the fault current level. In order to increase the fault level, one has to increase the capacity of the synchronous condenser so that its current contribution dominates in the combined short circuit current.

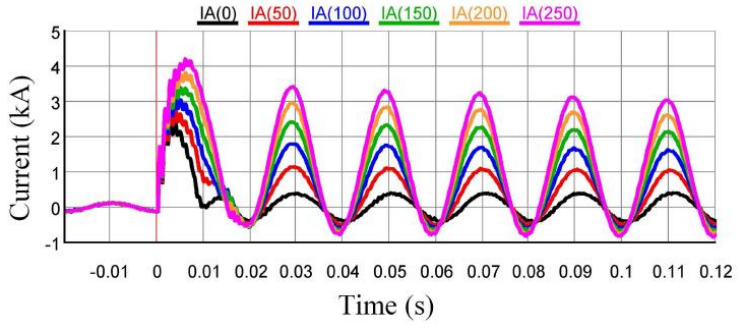

(a) Constant active power control for VSC1

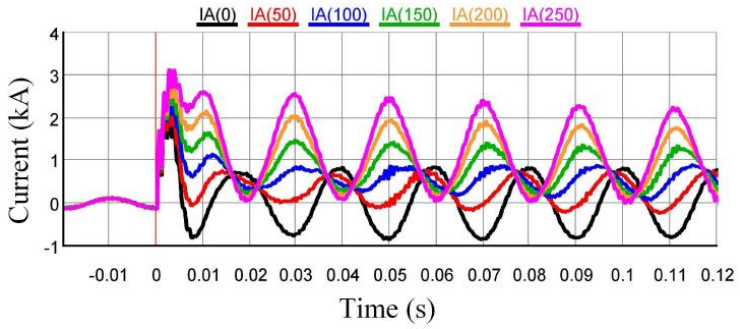

(b) Constant reactive power control for VSC1

Figure 29. Combined short circuit current from VSC and SC with different SC capacities under A-B fault

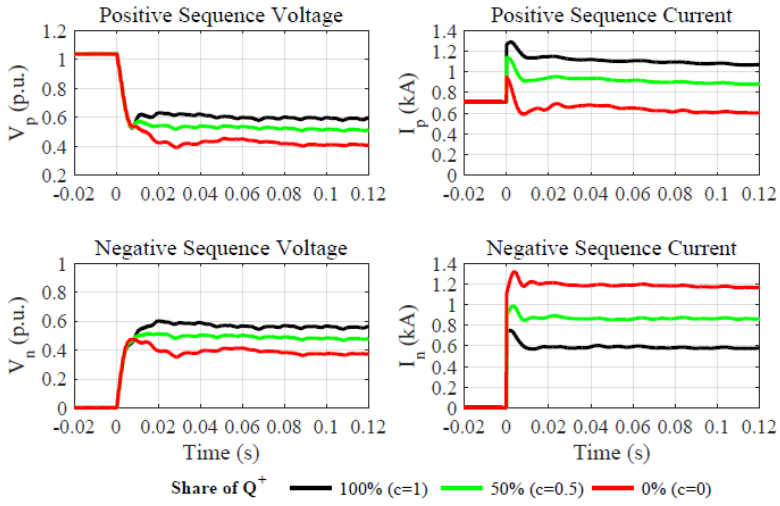

Figure 30. PCC voltage at bus 6 under A-B fault with different VSC control strategies

Figure 30 shows the sequence voltages at the PCC during faults with different VSC control strategies. Based on the voltage support concept, the sequence voltages are mainly affected by the sequence reactive powers for an inductive grid. For a VSC, it is active both in positive- and negative-sequence network. This is different from synchronous machines, which are passive in the negative-sequence network. They only provide a path for the negative-sequence current to flow through its impedance. Therefore, the effect of synchronous condnesrs on the PCC sequence voltages is not as notable as VSCs as shown in Fig. 31.

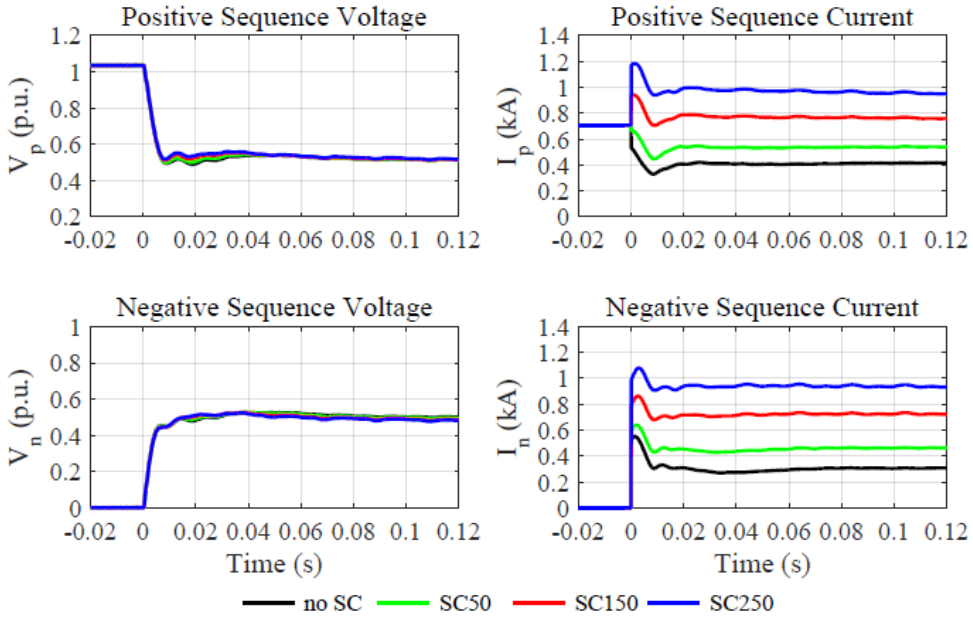

Figure 31. PCC voltage at bus 6 under A-B fault with capacities of SC

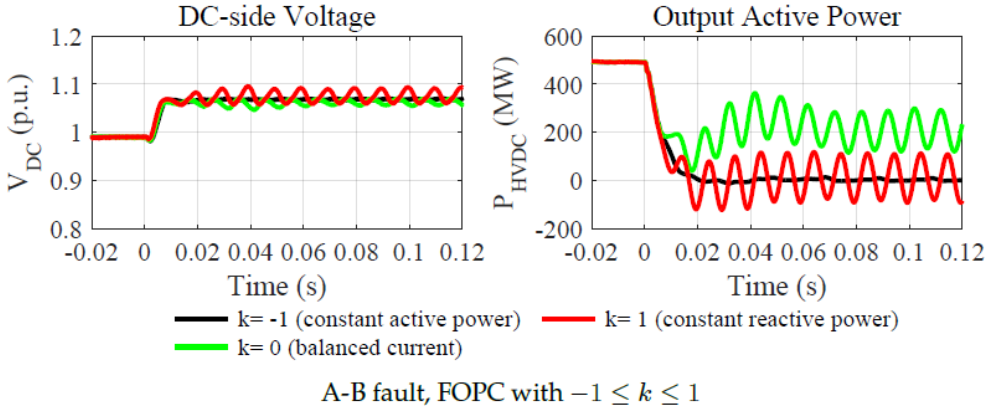

Figure 32. DC side voltage under A-B fault with different VSC control strategies

The DC side votlages of the VSC is mainly affected by the control strategies rather than the application of synchronous condensers. Different control strategies can result in different amplitudes of the oscillation on the DC-side. This is directly related to the oscillations in the output active power of the VSC. For example in Fig. 32, with the control strategy moving from constant active power control to constant reactive power control, there is an increase in the amplitudes of the DC-side voltage oscillations, as well as output active power oscillations. According to Fig. 27(c) which illustrates the relationship between FOPC and FPNSPC in an unified manner, the point (a, c) = (1, 1) represents that VSC1 provides only positive-sequence short circuit power (P+ and Q+). As long as the point moves away from (1,1), there will be negative-sequence current flowing through the converter. The further (a, c) is away from (1,1), the more negative-sequence current flows through the converter, which also means the more active power has to be curtailed in order not to violate the converter peak current limit. In this sense, the impact of the VSC1 control strategy on the system frequency response can be considered as a question of how much active power is curtailed during the fault. Based on the different scenarios shown in Fig. 33, it is concluded that: (1)

when there is under-frequency during the unbalanced fault, it is not recommended to have a < 1 because of two reasons. One is that the injection of positive P− occupies the converter current margin, leading to more active power to be curtailed. The second is that P− neither contributes to the voltage support for an inductive grid nor helps reduce the DC-side voltage oscillations. (2) On the other hand, when there is over-frequency during unbalanced faults, the injection of P− and Q− in both directions can help reduce the frequency deviation because of the active power curtailment. As a summary, Tab. 2 provides the guidelines on how to select control strategies for VSCs for a better application of synchronous condensers.

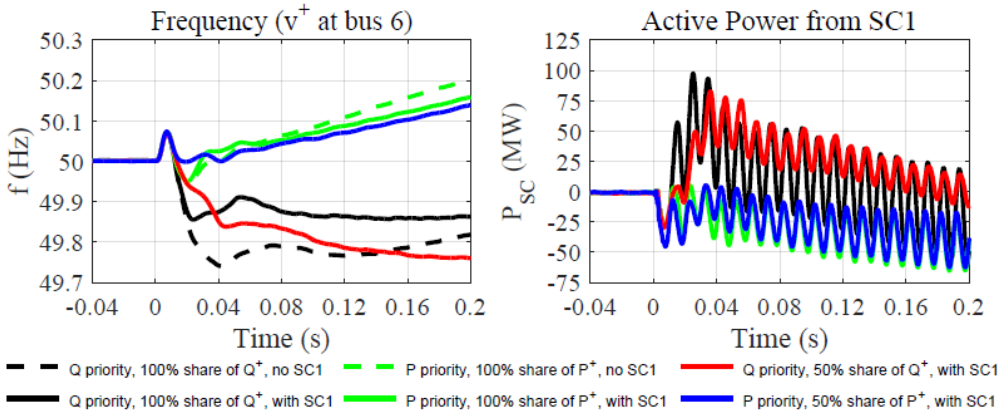

Figure 33. Frequency reponse under A-B fault with different VSC controls and SC.

Table 2. Guidelines on choosing VSC control strateiges for incorporating SC

Aspects	VSC dual-sequence current control	Synchronous condensers
Short circuit current	Avoid $k > 0$ with FOPC (can raise current cancellation problem);	Help bring the phases and amplitudes of the short circuit currents close to those from synchronous sources;
PCC voltage	(1) Affected by Q^+ and Q^- rather than P^+ and P^- for inductive grids; (2) The injection of positive Q^- ($k < 0$ with FOPC or $c < 1$ with FPNSPC) helps attenuate negative-sequence voltage;	Natural control on sequence-voltages;
DC-side voltage	(1) The injection of positive Q^- ($k < 0$ with FOPC or $0.5 < c < 1$ with FPNSPC) helps reduce DC-side voltage oscillations; (2) P^- has no notable effect	No notable effect;
Frequency response	(1) Affected by how much active power is curtailed; (2) For under-frequency, avoid the injection of positive P^- ($k > 0$ with FOPC or $a < 1$ with FPNSPC); (3) For over-frequency, the injection of P^- and Q^- in both directions helps counter frequency deviation;	Provide inertia for the system;

1.5.3.3 Assessment on distance protection

Distance protection is widely used in high-voltage transmission systems and serves as the backbone for the line protection. It uses the measured local voltage and current to calculate the apparent impedance seen from the relay location to the fault to decided if a fault is internal or external with respect to a protective zone. However, the short circuit response of VSCs deviates significantly from SGs. This can bring up challenges and pose threat to the reliability of distance protection for a future low inertia power system, where VSCs become the main sources of the short circuit current. Even though the potential impact of VSCs on distance

protection has raised much attention in recent years, less focus is given to unbalanced faults and the dual-sequence current controls of VSCs have been left unnoticed.

A distance relay typically has six measurement loops (A-g, B-g, C-g, A-B, B-C, and C-A), which will start to calculate the impedance after being released by the pickup method. For example, the circuit diagrams of the A-g loop under an A-g fault and the A-B loop under an A-B fault is illustrated in Fig. 34. As indicated, the existence of the fault resistance R introduces an error to the measured impedance and thus affects the reach of the line protection. This measuring error mainly depends on the pre-fault power flow (phase displacement between the voltage at the local termina and the remote terminal) in a conventional power system. It can be mitigated by adjusting the zone-inclination angle (tilting the reactance reach). However, with the presence of VSCs, whose short circuit current depends on the design of the control systems, the associated error can be enlarged and unpredictable so that the conventional compensation approach becomes insuffcient.

- A-B loop

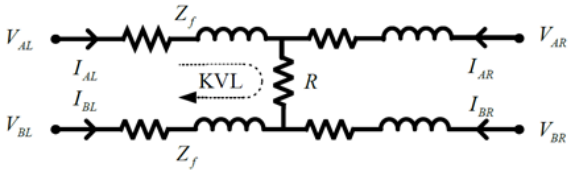

$$Z_{AB} = \underbrace{\frac{\dot{V}_{AL} - \dot{V}_{BL}}{\dot{I}_{AL} - \dot{I}_{BL}}}_{Measurement} = Z_f + R + \underbrace{R\frac{\dot{I}_{AR} - \dot{I}_{BR}}{\dot{I}_{AL} - \dot{I}_{BL}}}_{error}$$

- A-g loop

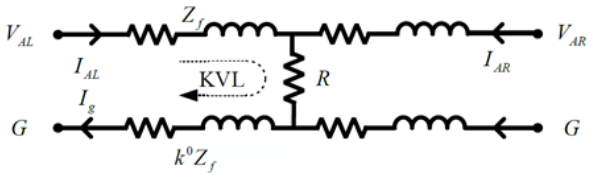

$$Z_{Ag} = \underbrace{\frac{\dot{V}_{AL}}{\dot{I}_{AL} + k^0 \dot{I}_g}}_{Measurement} = Z_f + R + \underbrace{R\frac{\dot{I}_{AR} - k^0 \dot{I}_g}{\dot{I}_{AL} + k^0 \dot{I}_g}}_{error}$$

Figure 34. Circuit diagrams for A-g and A-B faults.

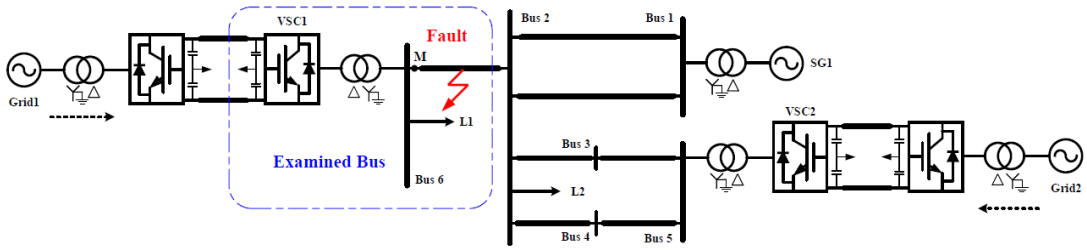

Figure 35. Test system.

Figure 35 presents the single-line diagram of the test system where the focus is given to Bus 6. The distance relay at point M protects the line from Bus 6 to Bus 2. The test is conducted through the hardware-in-the-loop test platform developed in this project.

As a base case, VSC1 is replace by a synchronous generator. Figure 36 shows the measured fault distance under different pre-fault power flow conditions and different values of fault resistance. It can be observed that the error caused by the fault resistance and the di erent pre-fault power flow conditions are not significant for such a synchronous-generator-dominated system. However, with the synchronous generators replaced by a VSC1 (active

power injection priority), there is significant overreaching problems if there is fault resistsnce as shown in Figure 37. The lower the available fault current, the large the errors is. On the other hand, if the VSC1 prioritize reactive power injection and has the ability to inject negative-sequenence current, both overreaching and underreaching problems can occur. This is jointly decided by the converter current limit level, fault resistance, pre-fault power flow conditions, and the control strategy as shown in Fig. 38.

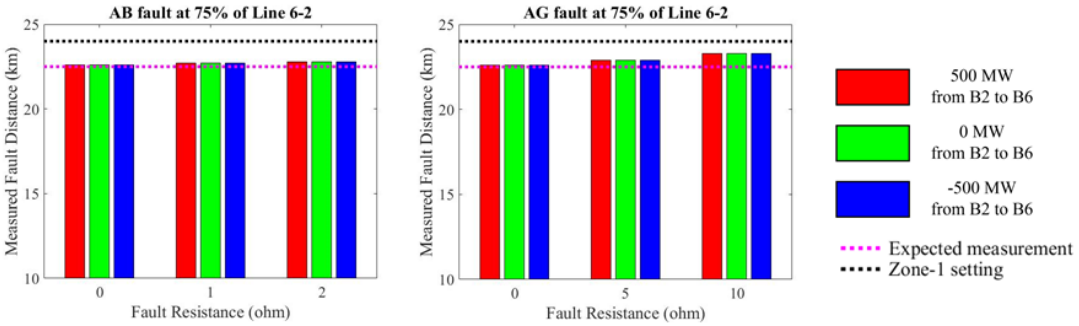

Figure 36. Measured fault distance with VSC1 placed by an SG.

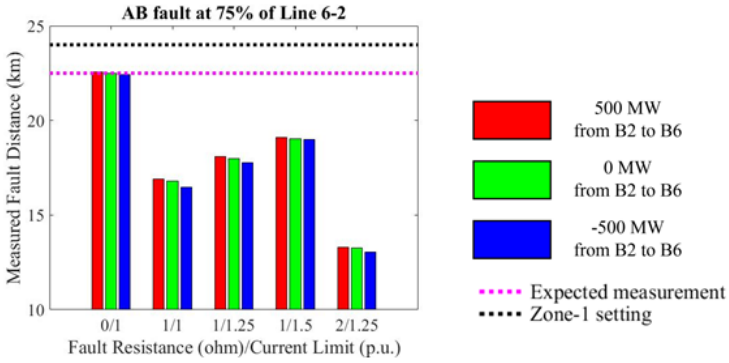

Figure 37. Measured fault distance with active power priority in VSC1.

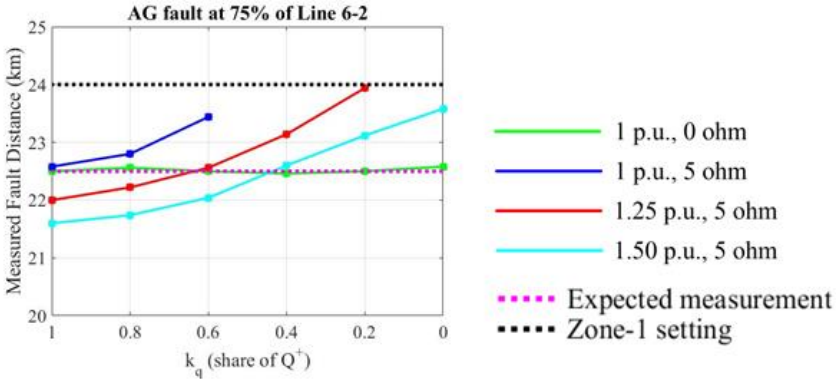

Figure 38. Measured fault distance with reactive power priority in VSC1 and different strategies.

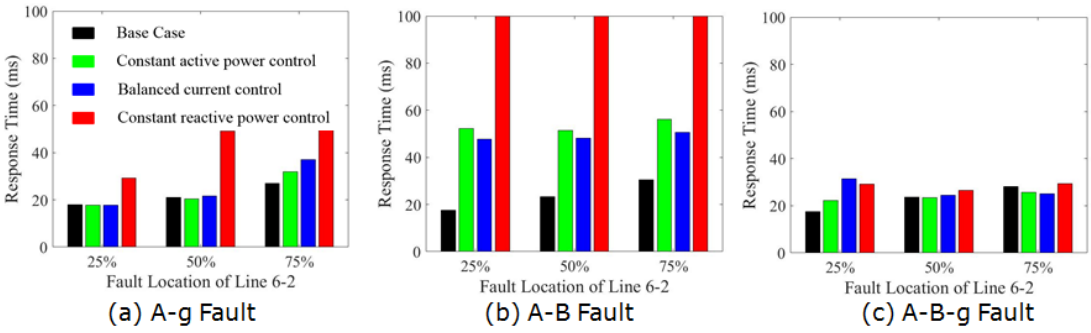

Figure 39. Average response time of the relay with different VSC1 control strategies.

Then the distance relay is further tested when VSC1 deploys FOPC control strategy. Figure 39 summarizes the average response time of the relay with respect to different fault types and locations. The response time with VSC1 generally increases when compared to the base case, especially for A-B faults. This indicates that the speed of distance protection may be jeopardized due to the low short circuit current level in low inertia power systems. For the three examined control strategies, constant active power control and balanced current control yield similar performances when it comes to the response time. Nevertheless, with VSC1 using constant reactive power control, the speed of the relay is deteriorated to a large extent for A-g faults. The relay even fails to trip under A-B faults. Figure 40 shows the impedance plane given by the relay for the A-B fault at 50% of line 6–2. More transients are observed in Fig. 40(b)–(c) than Fig. 40(a) before the locus stabilizes at the indicated fault location inside the zone. In Fig. 40(d), the impedance locus exhibits unfavorable features. The locus enters zone-1 without clearly indicating a fault location. The reason for this is that when constant reacticve power control is used, the fault current in phase A and B phase are exactly the same in both amplitude and phase. This introduce a zero value in the equation to calculate the A-B loop impedance. which cause the distance relay to be unable to calculate the impedance reliably. The same phenomenon in the A-B element can also be observed for A-B-g faults when using constant reactive power control. The operation of the distance relay under A-B-g faults relies on A-g, B-g, and A-B elements. Even though the relay can still operate successfully through the A-g and B-g elements, the use of constant reactive power control still pose threats to the reliability of the distance relay.

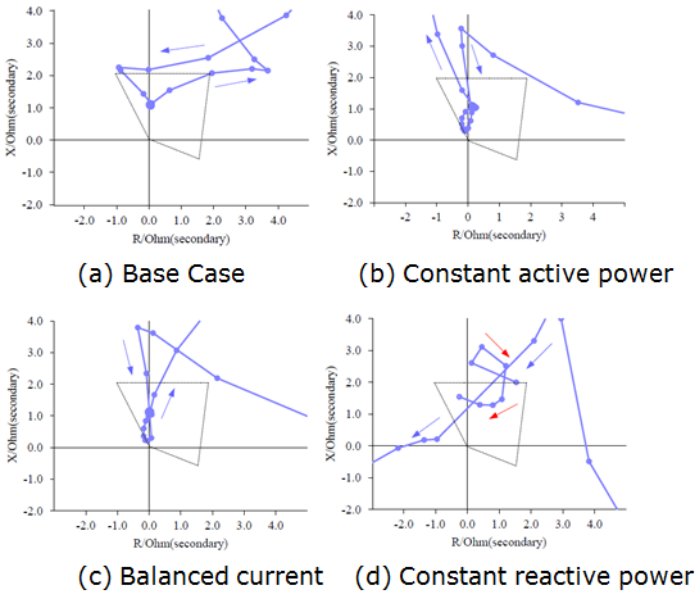

Figure 40. Impedance plane of the A-B element for the A-B fault at 50% of line 6-2.

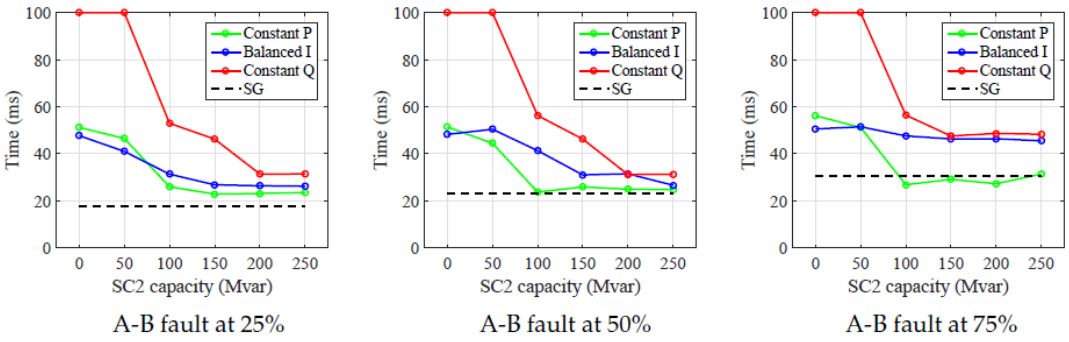

Figure 41. Average response time of distance relay with different SC capacities.

Next a synchronous condenser is added at the PCC, and thus the fault current is jointly provided by the VSC and the SC. With different types of fault and control strategies, Figure 41 shows the average response time of the distance relay in base case and with the presence of SC. When the capacity of SC1 increases from 0 to 250 Mvar, the speed of the distance relay improves generally and gets closer to base case. However, the relay still fails to trip with a 50 Mvar SC1 when constant reactive power control is used in VSC1. On the one hand, the short circuit current from a 50 Mvar SC1 is relatively small compared to that from the 500 MVA VSC1. On the other hand, as discussed above, there exists the current cancellation problem when using constant reactive power control strategy. As a result, the available short circuit current may be further reduced when using SC1 if the capacity of the SC and the control strategy of the VSC are not appropriate.

In conclusion, when active current injection is prioritized, the distance relay exhibited significant overreach problems. In contrast, both underreach and overreach problems arose when the priority was given to the reactive current. This uncertainty not only depends on the share of the injected positive-sequence reactive power, but also on the converter peak current limit level, the fault resistance, and the pre-fault power flow conditions. The test results revealed that the measuring error from the distance relay caused by the fault resistance can be enlarged in a future low inertia power system. The impact of the pre-fault power flow conditions on the reach also disagreed with the common knowledge for a conventional power system. These indeterminacies can make it difficult to do the relay settings and can jeopardize the effectiveness of the conventional countermeasures. Therefore, the non-pilot distance protection using the classic method may not be sufficient for serving as the primary protection of transmission lines. Protection studies should not ignore the converter peak current limit and the power electronics control, especially the dual-sequence current controls. The test results also showed that the reliability and speed of distance protection can be jeopardized because of the low short circuit current level and the non-conventional characteristics of the short circuit current, especially when VSCs are the main sources of the short circuit current. The application of a synchronous condenser at the PCC can help improve the relay performances, but this also relies on the dual-sequence current controls of the VSCs. It confirmed that FOPC with k > 0, especially constant reactive power control, should not be used together with distance protection. The associated current cancellation problem can cause the distance relay malfunction or can even reduce the available short circuit current. With the incorporation of a synchronous condenser at the PCC, constant active power control can be considered for the VSCs as its use requires a smaller synchronous condenser than balanced current control and constant reactive power control to retain distance relay performances.

1.5.3.4 Static fault analsysis method

The conventional fault analysis method for three-phase balanced faults sees that, the voltage change caused by the fault is equivalent to the voltage change caused by a voltage source (with the pre-fault voltage level) at the fault location if all other voltages sources are short-circuited. The fault analysis for unbalanced cases typically connects the sequence networks

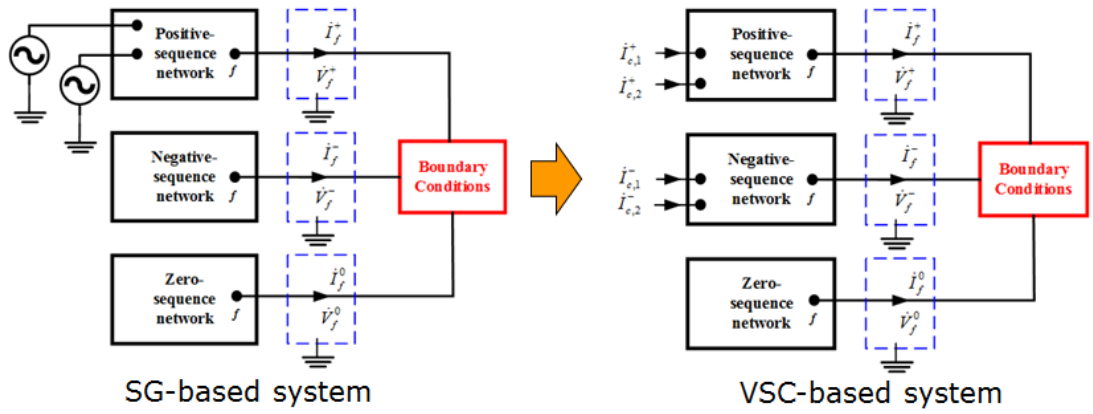

Figure 42. Transition of power system under fault conditions.

according to the boundary conditions defined by the fault types. However, with the presence of VSCs, the conventional fault analysis method is not sufficient. Firstly of all, VSCs are not natural voltage sources and their short circuit current depends on the control systems. In addition, the negativesequence current injection from VSCs under unbalanced faults turns the passive negative-sequence network into an active one. Considering the different control strategies, the magnitudes and phases of the actual currents is actually a function of the grid voltage. Moreover, according to the voltage support concept, the short circuit current from VSCs will also a ect the grid voltage. This means the actual grid voltage is a function of the short circuit current from VSCs. The dependency of voltage and current on each other indicates that an iterative method is necessary to perform the fault analysis.

This work developmed a new static fault analysis method that considering the presence of VSCs and their dual-sequence current control strategies. Conventionally, the fault current is provided by synchronous generators only in positive-sequence network, and the genrators can be modelled as ideal voltage sources behind impedances. However, as shown in Fig. 43, the future converter-based systems will have more current sources in both positive- and negative-sequence networks. Based on Fig. 43, synchronous sources are converterd into their equivalent Norton's circuits from the voltage source models, and VSCs are considered voltage-dependent current sources. Then superposition method is used. In the normal network, the fault current injection will raise the voltage in all the buses (Vf). In faulty networks, the flowing of fault current among different sequence networks will cause voltage drops. Therefore, by solving the circuit diagrams shown in Fig. 43, one can calculate the static fault current and then estimate how much voltage is retained during fault conditions under different types of faults.

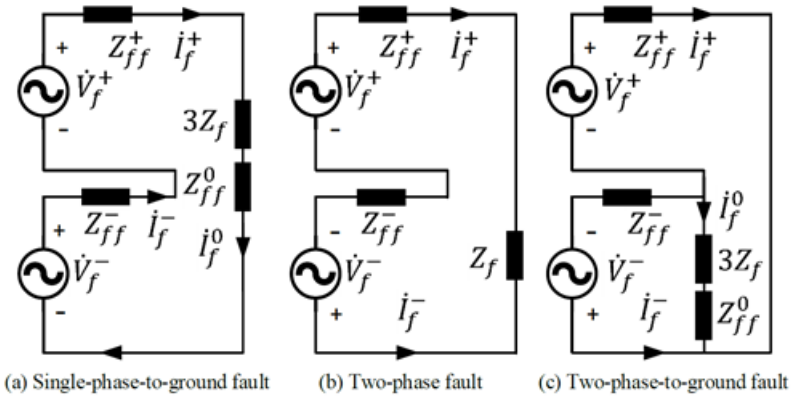

Figure 43. Boundary condition of sequence networks under unbalanced faults.

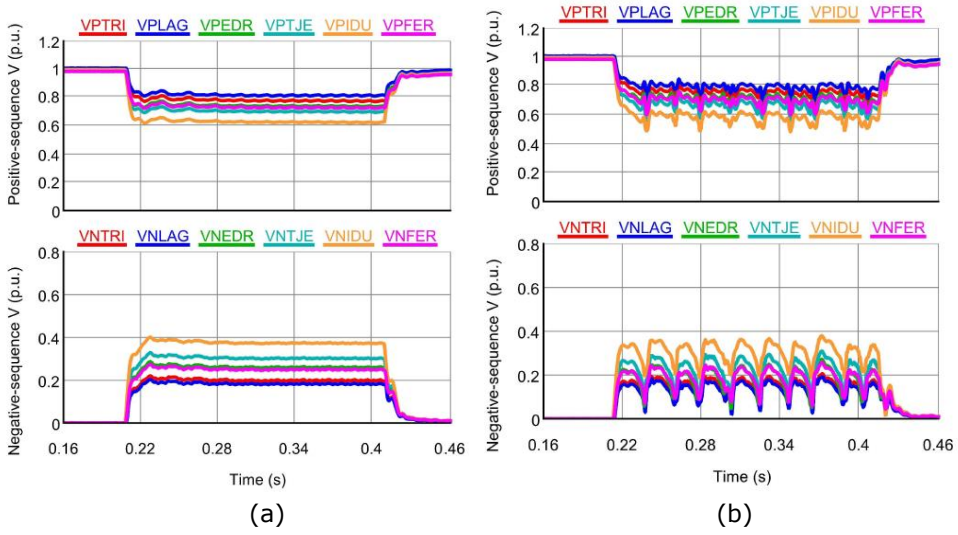

Figure 44. RTDS simulation of a large system with multiple VSCs.

Figure 44 shows sequence votlages of a large power system under unbalanced faults obtained by RTDS simulation. With the proposed method, one can calculate the retained voltage during faults in Fig. 42(a). However, if the control strategies of two VSC-HVDC converters are changed, the RTDS simulation does not give stable response as shown in Fig. 44(b). This is a new instability phenomen that has not been revealed in the literature. At this point, an assumpotion is made that the system does not exist an operating point. In order to further explore the reason and find an theoretical explanation, the proposed fault fault analsysi method is converted into an optimization problem. Mathematically speaking, the value of the defined objective function should be zero when the solution to the equation set, if existed, is substituted back. Therefore, the value of minimum value of the objection function (min(Z)) can serve as an indicator on if the equation set has a solution.

For the same system, Figure 45 presents the values of min(Z) with respect to the different combinations of c1 and c2 (the share of Q+ out of Q during faults). The scenarios marked by a red or a green dot has the value of min(Z) below 0.0001. The corresponding simulations in RTDS regarding these scenarios have a stable response like Fig. 44(a) during the fault. In contrast, with the rest of the combinations without being marked by a dot, the values of min(Z) are above 0.0001 and oscillatory behavior like Fig. 44(b) are observed in the RTDS simulations. It can be observed from Fig. 45 that, with the share of Q+ gradually decreasing, min(Z) gets further away from zero. This proves that the injection of Q− can lead to unstable responses during unbalanced faults, which is because the system does not have a stable operating point fulfilling the reactive power support and the equations of the fault analysis method. If the VSCs are controlled to provide negative-sequence current, the negative-sequence network. during a fault will become active. The simultaneous injection of Q+ and Q− can alter the positiveand negative-sequence voltages respectively at the PCC for an inductive grid. Since the current references of a VSC depend on the grid voltage, this will in return change the amplitudes and the phases of the current references. On top of that, the faulted network is also restrained by the boundary conditions. Therefore, the system may not have a stable operating point fulfilling all of these restrictions.

With three more synchronous generator phased out, it can also be observed that, the surface in Fig. 45(b) is further away from zero and gives fewer stable scenarios than Fig. 45(a). This makes the reactive power from VSCs to have more impact on the system voltage so that the system tolerates less negative-sequence reactive power Q−. Based on the above investigation, the dual-sequence current control strategies of VSCs involving negative-sequence current injection should be re-evaluated for future low inertia power systems. If the amount of Q− from VSCs is not restricted properly, the system may not have a stable response during unbalanced faults. The proposed fault analysis can serve as a tool to evaluate this issue

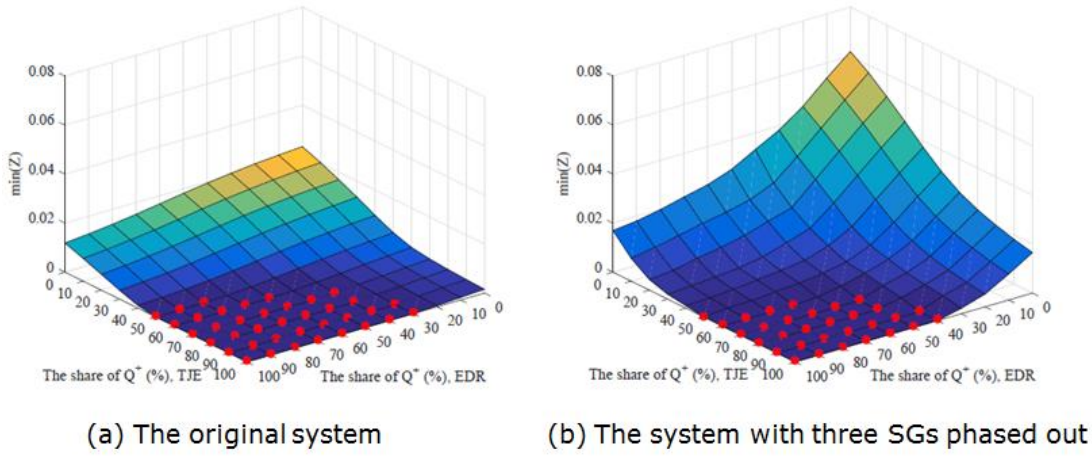

Figure 45. The values of min(Z) under different combinations of flexible scalars subject to an A-B fault

1.5.4 Hardware in loop test and validations

1.5.4.1 Hardware-in-the-loop test platform for protective relays

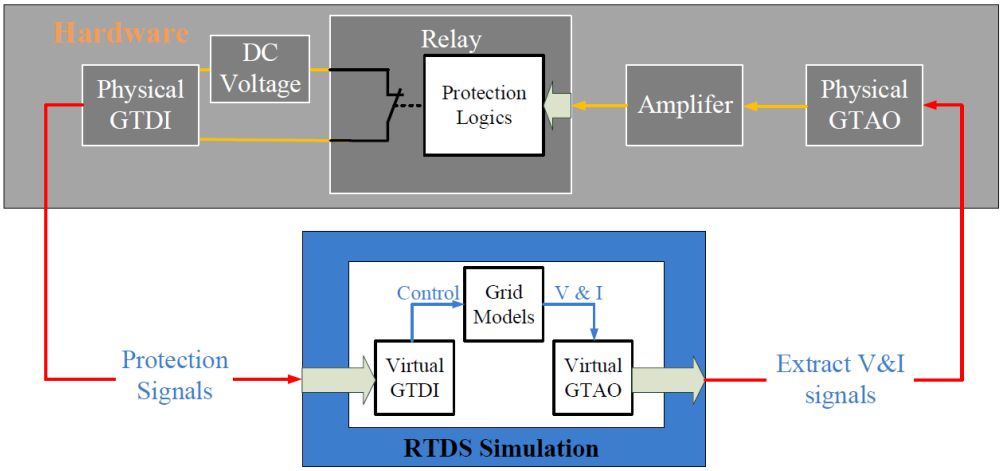

Figure 46. RTDS simulation with hardware

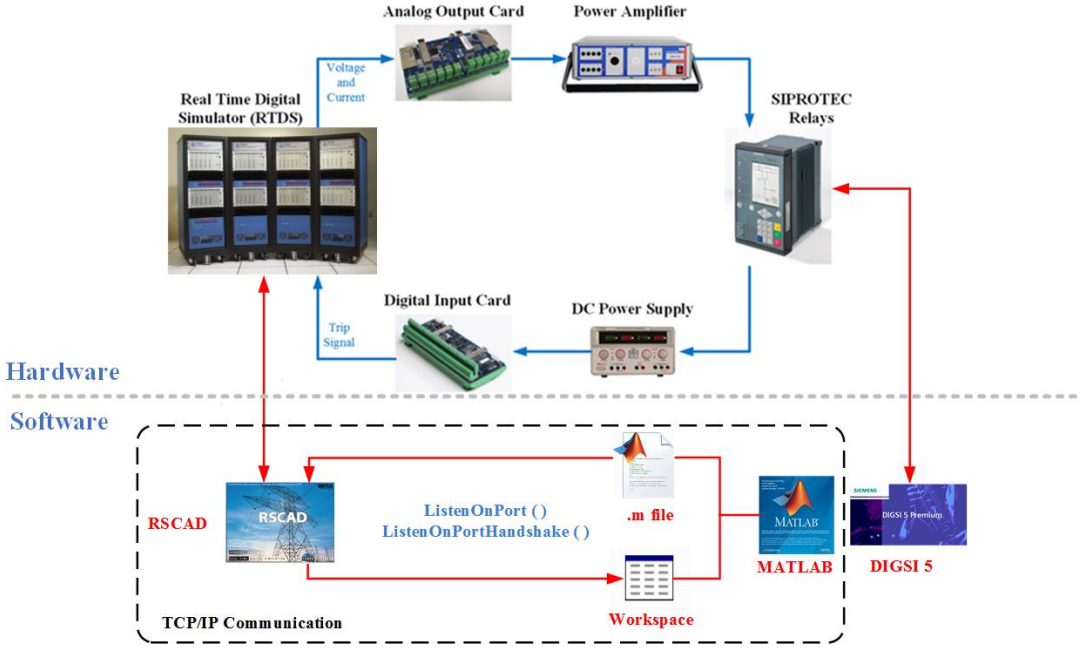

Figure 47. Hardware and software communications

In the SCAPP project, a HIL test platform illustrated by Fig. 46-47 is developed integrating power system models and real protective relays into a closed loop. As shown in Fig. 46 the power system model is simulated in RTDS, which sends out the three-phase voltage and current signals needed by the protective relay through a Gigabit Transceiver Analogue Output Card (GTAO). Given the fact that the output voltage of the GTAOis restricted to +/-10 V, the signals measured from the secondary sides of the Current Transformer (CT) and Voltage Transformer (VT) in simulations have to be scaled down properly through the output scaling factor of the virtual GTAO component in the simulation model. Then, an amplifier scales up the signals measured from the physical GTAO terminal so that amplified signals reach the level as obtained from the CT and VT. The trip signal generated by the relay is sent back to RTDS through a Gigabit Transceiver Digital Input Card (GTDI). When there is no current driven through its terminal, the digital input read by the RTDS processor card will be a logic "0". In order to have a logic "1", an external 5 V DC signal is needed to drive a current into the physical GTDI terminal. Since the protective relays used in the SCAPP project have potential-free switches, a 5 V DC voltage source is connected in series with the relay and the

physical GTDI. Therefore, a logic "1" will be registered if the switch of the relay closes, meaning the trip signal is sent from the relay to the RTDS simulations.

In addition, the HIL test platform integrates a TCP/IP link between RTDS and MATLAB. This bi-directional communication enables to automate the simulations, the relay testing, and the data saving by executing RSCAD/Runtime and Matlab. As a result, the platform can perform a large number of tests with various scenarios without the need of manual controls.

In the HIL test platform, the relay is configured through the SIPROTEC Relay kit software DIGSI 5. It acts as an interface between the user and the protective relay. The kit software is able to configure the routing of the relay inputs/outputs, select the protection schemes, specify the relay settings, monitor the device online, etc. The fault records are automatically saved in the relay and can be exported for further analysis. Some crucial aspects of the relay configuration are briefly described as follows:

- Select the correct device that matches with the physical relay from the library. Create the single-line diagram of the bay and associate the relay with the power system through the CT, the VT, and the circuit breaker. This single-line diagram can also be configured to be shown on the relay display.
- Specify the measuring-points routing and information routing. This is to guarantee that the inputs/outputs of the relay are assigned correctly to the desired terminals.
- Select the desired protection function and specify the settings of the relay. The "power system" setting mainly relates to the measurement supervision, while "Line 1" (distance protection in this case) relates to the actual setting of the protection schemes.

1.5.4.2 Optimal allocation of synchronous condensers

Synchronous condensers, as synchronous machines in principle, can contribute large amount of short circuit current and improve the system SCRs. The allocation of SCs in this section is formulated into an optimization problem. It decides the optimal locations and sizes of the new SCs so that the SCR of each converter terminal is maintained above a certain level while minimizing the total cost. This can be formulated into a Mixed-Integer Non-Linear Programming (MINLP) problem. In the proposed method, a binary variable is used to represent if a new SC should be installed at a certain location (1: installed; 0: not installed). An integer variable is used to scale the capacity of synchronous condeners so that the size can be involved in the optimization. Figure 48 shows the flow chart of the optimization using the proposed static fault analysis method.

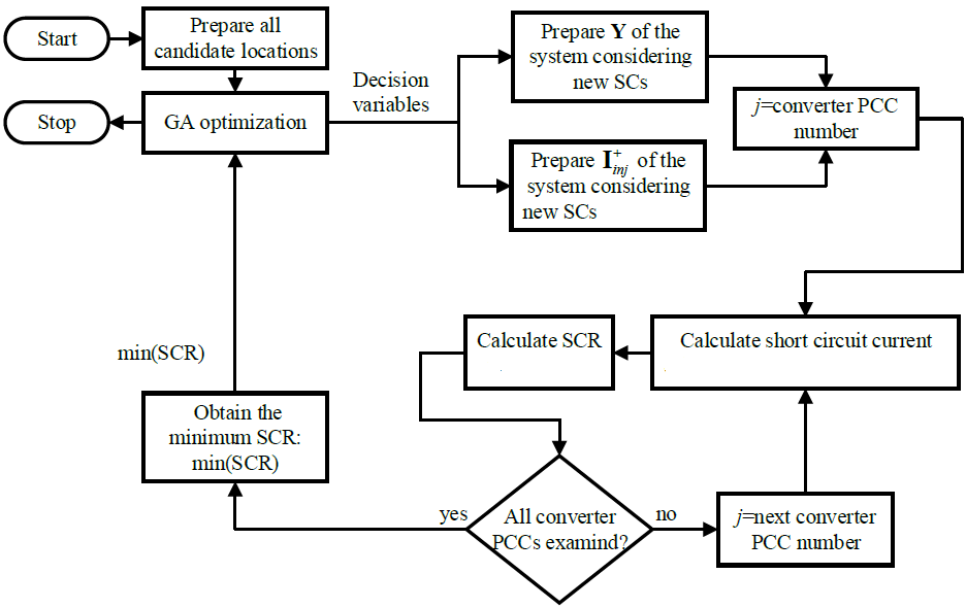

Figure 48. Flow chart of optimal allocation of synchronous condensers.

This work allocation synchronous condensers for the future western Danish power system shown in Fig. 49. The model corresponds to the transmission system covering the geographical area of Jylland and Fyn in Denmark with newly planed lines. The data for the synchronous machines, transformers, transmission lines and the system topology are provided by the Danish TSO Energinet. In Fig. 49, each substation at the 400 kV level is assigned a three-letter name. The entire power system together with its control systems is modeled in RTDS with details. Some key components in the model are:

- Three LCC-HVDC links at TJE, VHA and FGD to Norway, Sweden and Sjælland (DK2), respectively;
- Two VSC-HVDC links at TJE and EDR to Norway and The Netherlands, respectively;
- Two Type-III wind farms at KAE and TRI, respectively;
- One Type-IV wind farm at EDR;
- Five SGs at EDR, NVV, SVS, TRI and FYO, respectively;
- Three SCs at TJE, VHA and FGD, respectively;

In order to validate the RTDS model of the DK1 system, the real fault data is compared to the simulated short circuit response subject to the same fault. The simulated short circuit response agrees with the real fault data and this helps validate the RTDS model of the DK1 system.

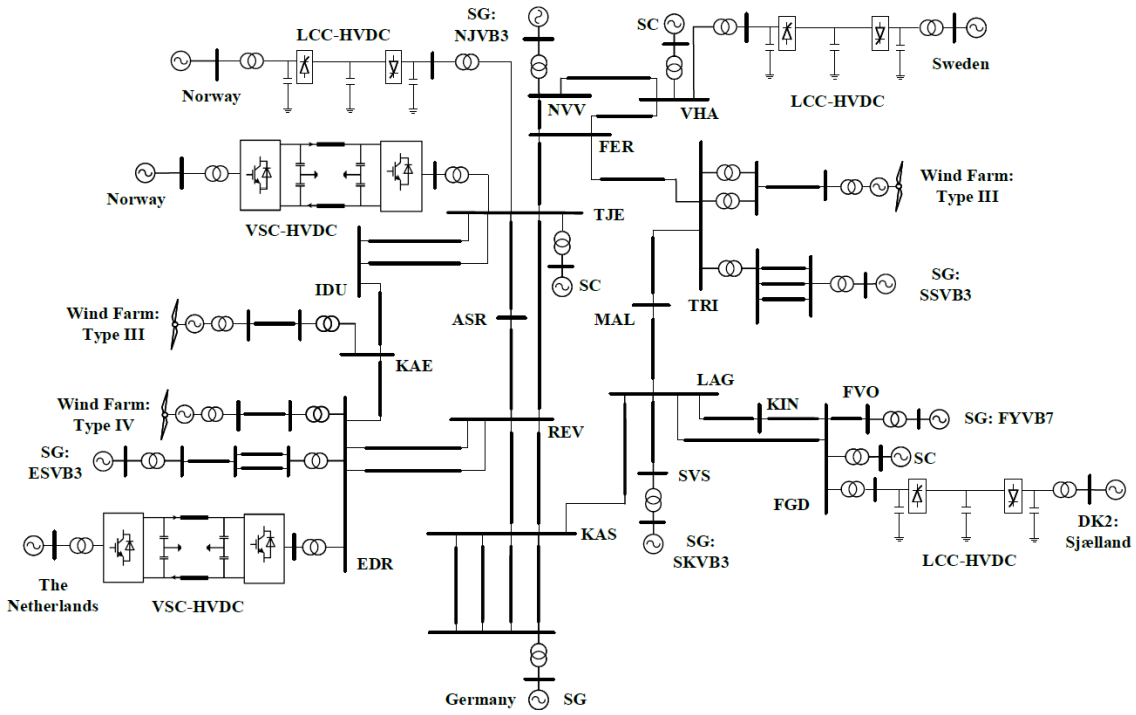

Figure 49. Single-line diagram of the future simplified wester Danish power system

Table 3. Installed capacity of HVDC systems and wind farms

Location	Total installed capacity
TJE	1000 MVA LCC-HVDC + 750 MVA VSC-HVDC
KAE	2×440 MVA Type-III wind farms
TRI	2×440 MVA Type-III wind farms
EDR	700 MVA VSC-HVDC + 3×400 MVA Type-IV wind farms
VHA	740 MVA LCC-HVDC
FGD	600 MVA LCC-HVDC
IDU	3×400 MVA Type-IV wind farms

For the purpose of allocation SCs for a future scenario, the following assumptions are made:

- The five SGs (ESVB3, NJVB3, SKVB3, FYVB7, and SSVB3) are phased out;
- The short circuit contribution from Germany is neglected;
- A new Type-IV wind farm is integrated at IDU;
- The installed capacity of the HVDC systems and wind farms is in accordance with Tab. 3;

Taking the short circuit contributions from VSC-based sources into account, it is assumed that all the VSC-HVDC systems and Type-IV wind farms inject 1 p.u. reactive current with respect to their own ratings under grid balanced faults while LCC-HVDC systems do not contribute any short circuit current under grid balanced faults. For the optimal SC allocation, two different sets of candidate SC locations are considered:

- Set 1: all 400 kV buses;
- Set 2: only converter terminals (PCCs) at 400 kV level;

The allocation results are summarized into Table 4 when the minimum short circuit ratio (SCR) is set to 3 and 4. For the case with M = 3, no feasible solution can be found with N = 1 (one SC allowed) for set 1 and set 2. When there is N = 2 (two SCs allowed), the optimization successfully generates six different solutions (plan 1–6) with the same costs. Since set 2 is the subset of set 1, plan 5 and plan 6 for set 1 can also be obtained for set 2. Figure 50(a) shows the SCRs at the PCCs with plan 1–6. It can be seen that EDR and TJE are the weakest points in the original system and their SCRs are below 3. With the planned SCs, the SCRs at TJE and EDR increase to at least 3, fulfilling the constraint of M = 3. For the case with M = 4, no feasible solution can be found with N = 1–4 for set 1. When there is N = 5 (five SCs allowed), the optimization successfully generates two di_erent solutions (plan 7–8) with the same costs. In contrast with set 2, no feasible solution can be found even when all the seven candidate locations are equipped with an SC of 270 Mvar (plan 9). The SCR at EDR is still below 4 as shown in Fig. 50(b). If the capacity of the available SCs increases to 500/250 Mvar, the optimization generated one solution (plan 10) when there is N = 5. The results from plan 7–10 indicate that the converter terminals may not always be the optimal locations for new SCs. When an SC is located at the PCC, it mainly helps increase the PCC locally rather than the other PCCs if the SC is relatively far away from the other converters in terms of electrical distance. However, if an SC locates somewhere between two PCCs properly, the SCRs at both PCCs can be improved simultaneously. Otherwise, larger SCs or more SCs are in need if only converter terminals are the candidate locations, which will also result in a higher cost.

Table 4. Synchronous condenser allocation plans

Minimum SCR	Set	Plan	Location and Rating [Mvar]	Cost [M$]	Note
3	1	1	EDR(270), REV(135)	14.15	with 270/135 Mvar SC
		2	EDR(135), REV(270)	14.15	
		3	EDR(270), ASR(135)	14.15	
		4	EDR(135), ASR(270)	14.15	
		5	EDR(270), KAE(135)	14.15	
		6	EDR(135), KAE(270)	14.15	
	2	5	EDR(270), KAE(135)	14.15	
		6	EDR(135), KAE(270)	14.15	
4	1	7	TJE(270), EDR(270), KAE(270), REV(270), ASR(270)	45.50	
		8	IDU(270), EDR(270), KAE(270), REV(270), ASR(270)	45.50	
	2	9	IDU(270), TJE(270), KAE(270), TRI(270), EDR(270), VHA(270), FGD(270)	63.70	with 270/135 Mvar SC, SCR at EDR is still below 4
		10	TJE(500), KAE(500), EDR(500), VHA(500), FGD(500)	80.00	with 500/250 Mvar SC

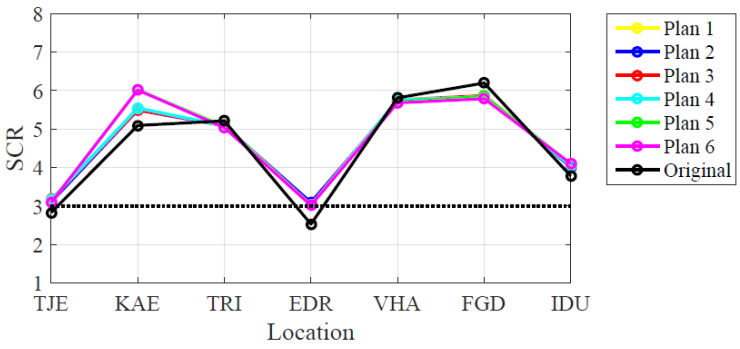

(a) with minimum SCR set to 3 (M=3)

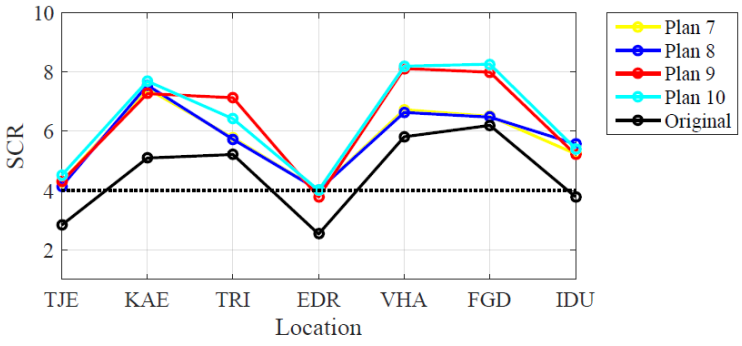

(b) with minimum SCR set to 4 (M=4)

Figure 50. Comparisons on system SCRs with different SC allocation plan.

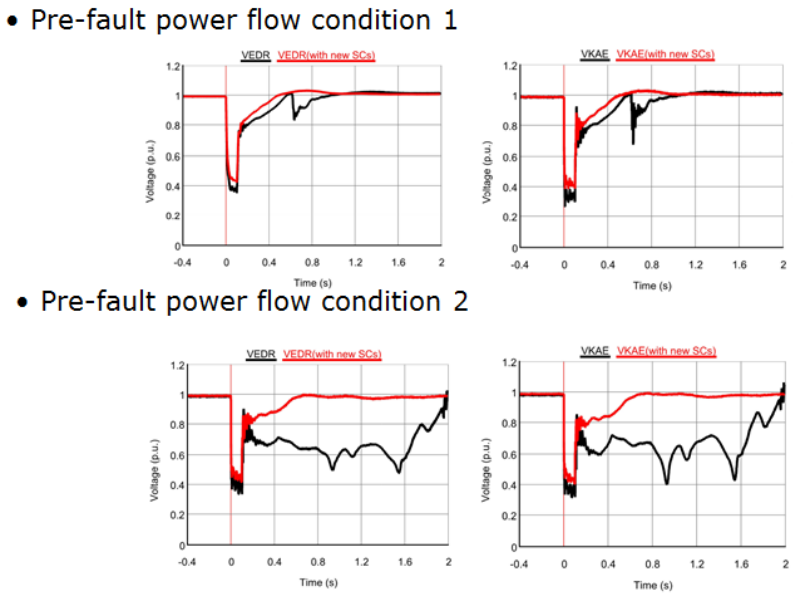

Figure 51. Comparisons on the voltage profiles before and after newly planed SCs.

In order to illustrate the effect of synchronous condensers, the voltages of the DK1 system are examined in RTDS without and with the new SCs from plan 5. Prior to the fault, all five SGs (ESVB3, NJVB3, SKVB3, FYVB7, and SSVB3) are disconnected from the grid and the grid in the German side is represented by an SG. All HVDC systems and wind farms are in operation according to the two different pre-fault conditions. During the fault, VSC-HVDC systems and Type-IV wind farms are controlled to inject 1 p.u. reactive current with respect to their own ratings. At the zero time instant, a solid three-phase balanced is initiated at ASR and the fault lasts for 0.1 s. Figure 51 compares the voltages at ASR, EDR, KAE and TJE without and with the two SCs at EDR (270 Mvar) and KAE (135 Mvar). It can be observed from Fig. 32 that system with two more SCs exhibits better fault-ridethrough performances than the original system. With the help of the two more SCs, the system has higher retained voltages

during the fault and has improved voltage profiles after the fault is cleared. For condition 2 where there is a higher power generation from the wind farms, the system is even not able to recover after the fault is cleared and the RTDS cannot run the whole system stably. In contrast, the added SCs help with the voltage recovery. The system maintains a stable operation after the fault is cleared.

1.6 Utilization of project results

The project results have been disseminated by various publications and educational activities. The project has successfully attracted industrial attentions. The work has been recognized as pioneer in the field and the study in the project has been widely referred in the industry as evidence of the effect of synchronous condensers to the grids with more renewables. There have been emails from grid operators and manufacturers asking for information regarding the published methods in the articles, stating finally there have been studies from academia where they can directly refer and use. Several transmission system operators from US, Australia and UK has contacted the project for further information.

The work is further continued afterwards by Ofgem (UK system operator) funded industrial led project Phoenix, as to the pioneering work done by DTU.

Publications	**Status**
[1]. Jundi Jia, Guangya Yang, Arne Hejde Nielsen, Vahan Gevorgian, "Investigation of short circuit power interaction between synchronous and VSC-based sources under grid unbalanced faults", IEEE Transactions on Power Delivery. doi: 10.1109/TPWRD.2019.2914342.	Published
[2]. Jundi Jia, Guangya Yang, Arne Hejde Nielsen, Peter Rønne-Hansen, "Hardware-in-the-loop tests on reverse power and frequency protection for synchronous condensers", CIGRE International Symposium Aalborg, Denmark, June 2019.	Published
[3]. H. T. Nguyen, G. Y. Yang, A. H. Nielsen, Peter-Højgaard Jensen, "Damping Frequency Oscillation in a Low Inertia System via the Control of Synchronous Condensers", IEEE Transactions on Power Systems.	To be submitted
[4]. H. T. Nguyen, G. Y. Yang, A. H. Nielsen, Peter-Højgaard Jensen, "Hardware- and Software-in-the-loop Simulation for Parameterizing the Model and Control of Synchronous Condenser", IEEE Transactions on Sustainable Energy, vol. 10, no. 3, pp. 1593-1602, July 2019. doi: 10.1109/TSTE.2019.2913471	Published
[5]. Jundi Jia, Guangya Yang, Arne Hejde Nielsen, Peter Rønne-Hansen, "Impact of VSC Control Strategies and Incorporation of Synchronous Condensers on Distance Protection under Unbalanced Faults", IEEE Transactions on Industrial Electronics, DOI: 10.1109/TIE.2018.2835389.	Published
[6]. H. T. Nguyen, G. Y. Yang, A. H. Nielsen, Peter-Højgaard Jensen, "Combination of Synchronous Condenser and Synthetic Inertia for Frequency Stability Enhancement in Low Inertia Systems", IEEE Transactions on Sustainable Energy, DOI: 10.1109/TSTE.2018.2856938	Published
[7]. Jundi Jia, G. Y. Yang, A. H. Nielsen, "Fault Analysis Method Considering Dual-Sequence Current Control of VSCs under Unbalanced Faults", Energies, DOI: 10.3390/en11071660.	Published
[8]. Jundi Jia, G. Y. Yang, A. H. Nielsen, Peter Rønne-Hansen "Study of control strategies of power electronics during faults in microgrids", book chapter in Hybrid-Renewable Energy Systems in Microgrids, Elsevier, Jun 2018. DOI: 10.1016/B978-0-08-102493-5.00007-8	Published
[9]. Sujay Ghosh, Kanakesh Vatta Kkuni, Guangya Yang, Lukasz Kocewiak, "Impedance scan and characterization of Type 4 wind power plants through ag-	Accepted

gregated model", accepted by IECON 2019.

[10]. Jundi Jia, G. Y. Yang, A. H. Nielsen, Peter Rønne-Hansen "Hardware-in-the-loop Tests on Distance Protection Considering VSC Fault-ride-through Control Strategies", IET the 14th International Conference on Development in Power System Protection (DPSP), UK, Mar. 2018. Published

[11]. Jundi Jia, G. Y. Yang, A. H. Nielsen, Peter Weinreich-Jensen, Eduard Muljadi, Vahan Gevorigian, "Synchronous Condenser Allocation for Improving System Short Circuit Ratio", The 5th International Conference on Electric Power and Energy Conversion Systems, Japan, Apr. 2018. Published

[12]. Ha Thi Nguyen, Guangya Yang, Arne Hejde Nielsen, Peter Højgaard Jensen, "Hardware-in-the-Loop Test for Automatic Voltage Regulator of Synchronous Condenser", 20th International Conference on Power Systems and Energy Conversion, Japan, Mar. 2018. Published

[13]. Cesar Guerriero, Ha Thi Nguyen, Guangya Yang, Tariq Rahman, Christopher Bolton, Peter Hojgaard Jensen, "Talega SynCon - Power Grid Support for Renewable-based Systems", IEEE/PES Transmission and Distribution Conference and Exposition (T&D), 2020. Published

[14]. Ha Thi Nguyen, Guangya Yang, Arne Hejde Nielsen, Peter Højgaard Jensen, C. F. Coimbra, "Frequency Stability Improvement of Low Inertia Systems Using Synchronous Condensers", IET the 7th International Conference on Renewable Power Generation, Denmark, Sep. 2018. Published

[15]. Jundi Jia, Guangya Yang, Arne Hejde Nielsen, "A Review on Grid-connected Converter Control for Short Circuit Power Provision under Grid Unbalanced Faults", IEEE Transactions on Power Delivery, DOI: 10.1109/TPWRD.2017.2682164. Published

[16]. Emanuel Marazzi, Guangya Yang, Peter Weinreich-Jensen, "Allocation of Synchronous Condensers in Low Inertia Systems: A Danish case study", Journal of Modern Power System and Clean Energy, DOI: 10.1007/s40565-017-0346-4. Published

[17]. Moumita Sarkar, Jundi Jia, Guangya Yang, "Distance relay performance in low inertia systems", IEEE PowerTech Conference, UK, Jun. 2017. Published

[18]. Jundi Jia, G. Y. Yang, A. H. Nielsen, "Investigation of Grid-connected Voltage Source Converter Performance under Unbalanced Fault", IEEE PES Asia-Pacific Power and Energy Engineering Conference, China, Oct. 2016. Published

[19]. Ha Thi Nguyen, Guangya Yang, Arne Hejde Nielsen, Peter Højgaard Jensen, Frequency Stability Improvement of Low Inertia Systems Using Synchronous Condensers, IEEE Smart Grid Communication Conference, Australia, Nov. 2016 Published

Presentations	**Status**
"Protection system performance in weak AC grids through HiL tests", presented at IEEE General Meeting 2017, Chicago.	Delivered
"Application of Synchronous Condensers in Low Inertia Systems from Danish project SCAPP reference group meeting", presented at reference group meeting DTU, 23 Jan 2017.	Delivered
"Synchronous Condenser – A Moderator in Renewable Energy Systems - From Danish project SCAPP", presented at Siemens CKI Conference at DTU, 22 Sept 2016.	Delivered
"Studies on low inertia systems and application of synchronous condensers",	Delivered

presented at IEEE Power Engineering Society General Meeting, July 17-21, Boston, MA, 2016.

Outreach	**Status**
"One step closer to 100 pct. renewable energy", CEE News (30 JAN 17), Online: http://www.cee.elektro.dtu.dk/news/nyhed?id=19CB0ABC-43E7-49D9-A0E0-D72E92C27BF9	Published
"Sol og vind på cruisekontrol", DTU News (12/Jul/2016), Reposted by Energy Supply DK. Online: http://www.energy-supply.dk/article/view/253017/sol_og_vind_pa_cruisekontrol#	Published

MSc projects	**Status**
Short circuit current characterization and incorporation of synchronous sources for wind power plants (2017/05 – 2017/11)	Finished
Technical and economic evaluation of inertia from wind farms and synchronous condensers (2017/02 – 2017/08)	Finished
Investigation of distance relay performance for blackout prevention in low inertia electric power systems (2016/02 – 2016/08)	Finished
Short circuit power planning for renewable energy systems via synchronous condensers (2015/01 – 2015/10)	Finished
Effect of VSC-HVDC on distance relay based on RTDS simulation (2015/01-2015/10)	Finished
Protection Schemes for High Voltage Systems. - Effect of Saturation in Current (2014/11 - 2015/08)	Finished
Evaluation of the impact of full converter wind turbine during faults on grid protections (2015/01-2015/07)	Finished
Allocation of synchronous condensers for low inertia systems (2015/01 – 2015/07)	Finished

1.7 Project conclusion and perspective

The project has successfully built a hardware in the loop platform linking real time simulation, AVR and protection system of SC for studying the effects of synchronous condensers in the future renewable energy system. In this regard, positive effects of SC on frequency and voltage have been verified. Innovative methods for using SC to damp power swings and analyzing converter based grids during faults are proposed. Further research can be in the following two areas,

1. Coordinated use of SCs for system stability enhancement;
2. Hybrid SC design such as SC+battery to provide multi-dimentional services;

The application of SCs can be promising in the future converter based systems, including low inertia or zero inertia (offshore multi terminal DC) grids, to provide short circuit power, dynamic voltage support, intrinsic inertia, and critical damping to the system. The application can be boosted if the need of such services can be recognized by the system operator, where a marketplace is created for service provision.